A chemical screen based on an interruption of zebrafish gastrulation identifies the HTR2C inhibitor Pizotifen as a suppressor of EMT-mediated metastasis

Joji Nakayama[1,2,3,4,§], Lora Tan[1], Boon Cher Goh[2], Shu Wang[1, 5], Hideki Makinoshima[3,6] and Zhiyuan Gong[1,§]

[1]Department of Biological Science, National University of Singapore, Singapore
[2]Cancer Science Institute of Singapore, National University of Singapore, Singapore
[3]Tsuruoka Metabolomics Laboratory, National Cancer Center, Tsuruoka, Japan
[4]Shonai Regional Industry Promotion Center, Tsuruoka, Japan.
[5]Institute of Bioengineering and Nanotechnology, Singapore
[6]Division of Translational Research, Exploratory Oncology Research and Clinical Trial Center, National Cancer Center, Kashiwa, Japan.

[§]Corresponding authors:
Joji Nakayama
email: Zmetastasis@gmail.com

Zhiyuan Gong
email: dbsgzy@nus.edu.sg

Keywords: Metastasis, gastrulation, EMT, Phenotyping screening, zebrafish

Total words excluding supplemental figure legends and references section: 5468

Number of figures: 5
Number of tables: 1
Number of supplemental figures: 3
Number of supplemental tables: 6

Abstract

Metastasis is responsible for approximately 90% of cancer-associated mortality but few models exist that allow for rapid and effective screening of anti-metastasis drugs. Current mouse models of metastasis are too expensive and time consuming to use for rapid and high-throughput screening. Therefore, we created a unique screening concept utilizing conserved mechanisms between zebrafish gastrulation and cancer metastasis for identification of potential anti-metastatic drugs. We hypothesized that small chemicals that interrupt zebrafish gastrulation might also suppress metastatic progression of cancer cells and developed a phenotype-based chemical screen to test the hypothesis. The screen used epiboly, the first morphogenetic movement in gastrulation, as a marker and enabled 100 chemicals to be tested in five hours. The screen tested 1280 FDA-approved drugs and identified Pizotifen, an antagonist for serotonin receptor 2C (HTR2C) as an epiboly-interrupting drug. Pharmacologic and genetic inhibition of HTR2C suppressed metastatic progression in a mouse model. Blocking HTR2C with Pizotifen restored epithelial properties to metastatic cells through inhibition of Wnt-signaling. In contrast, HTR2C induced epithelial to mesenchymal transition (EMT) through activation of Wnt-signaling and promoted metastatic dissemination of human cancer cells in a zebrafish xenotransplantation model. Taken together, our concept offers a novel platform for discovery of anti-metastasis drugs.

Introduction

Metastasis, a leading contributor to the morbidity of cancer patients, occurs through multiple steps: invasion, intravasation, extravasation, colonization, and metastatic tumor formation (1-3). The physical translocation of cancer cells is an initial step of metastasis and molecular mechanisms of it involve cell motility, the breakdown of local basement membrane, loss of cell polarity, acquisition of stem cell-like properties, and EMT (4-6). These cell-biological phenomena are also observed during vertebrate gastrulation in that evolutionarily conserved morphogenetic movements of epiboly, internalization, convergence, and extension progress (7). In zebrafish, the first morphogenetic movement, epiboly, is initiated at approximately 4 hours post fertilization (hpf) to move cells from the animal pole to eventually engulf the entire yolk cell by 10 hpf (8, 9). The embryonic cell movements are governed by the molecular mechanisms that are partially shared in metastatic cell dissemination.

At least fifty common genes were shown to be involved in both metastasis and gastrulation progression: Knockdown of these genes in Xenopus or zebrafish induced gastrulation defects; conversely, overexpression of these genes conferred metastatic potential on cancer cells and knockdown of these genes suppressed metastasis (Table S1). This evidence led us to hypothesize that small molecules that interrupt zebrafish gastrulation may suppress metastatic progression of human cancer cells.

Here we report a unique screening concept based on the hypothesis. Pizotifen, an antagonist for HTR2C, was identified from the screen as a “hit” that interrupted zebrafish gastrulation. A mouse model of metastasis confirmed pharmacological and genetic inhibition of HTR2C suppressed metastatic progression. Moreover, HTR2C induced EMT and promoted metastatic dissemination of non-metastatic cancer cells in a zebrafish xenotransplantation model. These results demonstrated that this concept could offer a novel high-throughput platform for discovery of anti-metastasis drugs and can be converted to a chemical genetic screening platform.

Results

Small molecules interrupting epiboly of zebrafish have a potential to suppress metastatic progression of human cancer cells.

Before performing a screening assay, we conducted preliminary experiments to test the hypothesis. First, we examined whether hindering the molecular function of reported genes, whose knockdown induced gastrulation defects in zebrafish, might suppress cell motility and invasion of cancer cells. We chose protein arginine methyltransferase 1 (PRMT1) and cytochrome P450 family 11 (CYP11A1), both of whose knockdown induced gastrulation defects in zebrafish but whose involvement in metastatic progression is unclear (10, 11). Elevated expression of PRMT1 and CYP11A1 were observed in highly metastatic human breast cancer cell lines and knockdown of these genes through RNA interference suppressed the motility and invasion of MDA-MB-231 cells without affecting their viability (Figure S1A-C).

Next, we conducted an inverse examination of whether chemicals which were reported to suppress metastatic dissemination of cancer cells could interrupt epiboly progression of zebrafish embryos. Niclosamide and Vinpocetine are reported to suppress metastatic progression (12, 13) (14, 15). Either Niclosamide or Vinpocetine-treated zebrafish embryos showed complete arrest at very early stages or severe delay in epiboly progression, respectively (Figure S1D).

These results suggest that epiboly could serve as a marker for this screening assay and epiboly-interrupting drugs that are identified through this screening could have the potential to suppress metastatic progression of human cancer cells.

132 FDA-approved drugs induced delayed in epiboly of zebrafish embryos

We screened 1,280 FDA, EMA or other agencies-approved drugs (Prestwick, Inc) in our zebrafish assay. The screening showed that 0.9% (12/1280) of the drugs, including Actimycin A and Tolcapone, induced severe or complete arrest of embryonic cell

102 movement when embryos were treated with 10μM. 5.2% (66/1280) of the drugs, such as
103 Dicumarol, Racecadotril, Pizotifen and S(-) Eticlopride hydrochloride, induced either
104 delayed epiboly or interrupted epiboly of the embryos. 93.3% (1194/1280) of drugs has
105 no effect on epiboly progression of the embryos. 0.6% (8/1280) of drugs induced a toxic
106 lethality. Epiboly progression was affected more severely when embryos were treated
107 with 50μM; 1.7% (22/1280) of the drugs induced severe or complete arrest of it. 8.6%
108 (110/1280) of the drugs induced either delayed epiboly or interrupt epiboly of the
109 embryos. 4.3% (55/1280) of drugs induced a toxic lethality (Figure 1A and 1B, Table S2).
110 Among the epiboly-interrupting drugs, several drugs have already been reported to inhibit
111 metastasis-related molecular mechanisms: Adrenosterone or Zardaverine, which target
112 HSD11β1 or PDE3 and 4, respectively, are reported to inhibit EMT (16, 17);
113 Racecadotril, which targets enkephalinase, is reported to confer metastatic potential on
114 colon cancer cell (18); and Disulfiram, which targets ALDH, is reported to confer stem-
115 like properties on metastatic cancer cells (19). This evidence suggests that epiboly-
116 interrupting drugs have the potential for suppressing metastasis of human cancer cells.
117
118 **Identified drugs suppressed cell motility and invasion of human cancer cells.**
119 It has been reported that zebrafish have orthologues to 86% of 1318 human drug targets
120 (20). However, it was not known whether the epiboly-interrupting drugs could suppress
121 metastatic dissemination of human cancer cells. To test this, we subjected the 78 epiboly-
122 interrupting drugs that showed a suppressor effect on epiboly progression at a 10μM
123 concentration to *in vitro* experiments using a human cancer cell line. The experiments
124 examined whether the drugs could suppress cell motility and invasion of MDA-MB-231
125 cells through a Boyden chamber. Before conducting the experiment, we investigated
126 whether these drugs might effect viability of MDA-MB-231 cells using an MTT assay.
127 Sixteen of the 78 drugs strongly effected cell viability at concentrations less than 1μM
128 and were not used in the cell motility experiments. The remaining 62 drugs were assayed

129 in Boyden chamber motility experiments. Twenty of the 62 drugs inhibited cell motility
130 and invasion of MDA-MB-231 cells without effecting cell viability. Among the 20 drugs,
131 Hexachlorophene and Nitazoxanide were removed since the primary targets of the drugs,
132 D-lactate dehydrogenase and pyruvate ferredoxin oxidoreductase are not expressed in
133 mammalian cells. With the exception of Ipriflavone, whose target is still unclear, the
134 known primary targets of the remaining 17 drugs are reported to be expressed by
135 mammalian cells (Figure 2A and Table 1).
136 We confirmed if highly metastatic human cancer cell lines expressed the genes
137 that code for these targets using Western blotting analyses. Among the genes, serotonin
138 receptor 2C (HTR2C), which is a primary target of Pizotifen, was highly expressed in
139 only metastatic cell lines (Figure 2B). Pizotifen suppressed cell motility and invasion of
140 several highly metastatic human cancer cell lines in a dose-dependent manner (Figure
141 2C). Similarly, Dopamine receptor D2 (DRD2), which is a primary target of S(-)
142 Eticlopride hydrochloride, was highly expressed in only metastatic cell lines, and the drug
143 suppressed cell motility and invasion of these cells in a dose-dependent manner (Figure
144 S2).
145 These results indicate that a number of the epiboly-interrupting drugs also have
146 suppressor effects on cell motility and invasion of highly metastatic human cancer cells.
147
148 **Pizotifen suppressed metastatic dissemination of human cancer cells in a zebrafish**
149 **xenotransplantation model.**
150 While a number of the epiboly-interrupting drugs suppressed cell motility and invasion of
151 human cell lines *in vitro,* it was still unclear whether the drugs could suppress metastatic
152 dissemination of cancer cells in vivo. Therefore, we examined whether the identified
153 drugs could suppress metastatic dissemination of these human cancer cells in a zebrafish
154 xenotransplantation model. Pizotifen was selected to test since HTR2C was overexpressed
155 only in highly metastatic cell lines supporting the hypothesis that it could be a novel target

156 for blocking metastatic dissemination of cancer cells (Figure 2B). Red fluorescent
157 protein-labelled MDA-MB-231 (231R) cells were injected into the duct of Cuvier of *Tg*
158 *(kdrl:eGFP)* zebrafish at 2 dpf and then maintained in the presence of either vehicle or
159 Pizotifen. Twenty-four hours post-injection, the numbers of fish showing metastatic
160 dissemination of 231R cells were measured via fluorescence microscopy. In this model,
161 the dissemination patterns were generally divided into three categories: (i) head
162 dissemination, in which disseminated 231R cells exist in the vessel of the head part; (ii)
163 trunk dissemination, in which the cells were observed in the vessel dilating from the trunk
164 to the tail; (iii) end-tail dissemination, in which the cells were observed in the vessel of
165 the end-tail part (16).

166 Three independent experiments revealed that the frequencies of fish in the drug-
167 treated group showing head, trunk, or end-tail dissemination, significantly decreased to
168 55.3±7.5%, 28.5±5.0% or 43.5±19.1% when compared with those in the vehicle-treated
169 group; 95.8±5.8%, 47.1±7.7% or 82.6±12.7%. Conversely, the frequency of the fish in the
170 drug-treated group not showing any dissemination, significantly increased to 45.4±0.5%
171 when compared with those in the vehicle-treated group; 2.0±2.9% (Figure 2D and Table
172 S3).

173 Similar effects were observed in another xenograft experiments using an RFP-
174 labelled human pancreatic cancer cell line, MIA-PaCa-2 (MP2R). In the drug treated
175 group, the frequencies of the fish showing head, trunk or end-tail dissemination,
176 significantly decreased to 15.3±6.7%, 6.2±1.3%, or 41.1±1.5%; conversely, the frequency
177 of the fish not showing any dissemination significantly increased to 46.3±8.9% when
178 compared with those in the vehicle-treated group; 74.5±11.1%, 18.9±14.9%, 77.0±9.0%,
179 or 17.2±0.7% (Figure S3 and Table S4).

180 To eliminate the possibility that the metastasis suppressing effects of Pizotifen
181 might result from off-target effects of the drug, we conducted validation experiments to
182 determine whether knockdown of HTR2C would show the same effects. Sub-clones of

183 231R cells that expressed shRNA targeting either LacZ or HTR2C were injected into the
184 fish at 2 dpf and the fish were maintained in the absence of drug. In the fish that were
185 inoculated with shHTR2C 231R cells, the frequencies of the fish showing head, trunk,
186 and end-tail dissemination, significantly decreased to 6.7±4.9%, 6.7±0.7%, or
187 20.0±16.5%; conversely, the frequency of the fish not showing any dissemination,
188 significantly increased to 80.0±4.4% when compared with those that were inoculated with
189 shLacZ 231R cells; 80.0±27.1%, 20.0±4.5%, 90.0± 7.7%, or 0% (Figure 2E and Table
190 S5).
191 These results indicate that pharmacological and genetic inhibition of HTR2C
192 suppressed metastatic dissemination of human cancer cells in vivo.
193
194 **Pizotifen suppressed metastasis progression of a mouse model of metastasis.**
195 We examined the metastasis-suppressor effect of Pizotifen in a mouse model of
196 metastasis (21). Luciferase-expressing 4T1 murine mammary carcinoma cells were
197 inoculated into the mammary fat pads (MFP) of female BALB/c mice. On day two post
198 inoculation, the mice were randomly assigned to two groups and one group received once
199 daily intraperitoneal injections of 10mg/kg Pizotifen while the other group received a
200 vehicle injection. Bioluminescence imaging and tumor measurement revealed that the
201 sizes of the primary tumors in Pizotifen-treated mice were equal to those in the vehicle-
202 treated mice at the time of resection on day 10 post inoculation. Immunofluorescent
203 staining also demonstrated that the percentage of Ki67 positive cells in the resected
204 primary tumors of Pizotifen-treated mice were the same as those of vehicle-treated mice
205 (Figure 3A-C), additionally, both groups showed less than 1% cleaved caspase 3 positive
206 cells (data not shown). Therefore, no anti-tumor effect of Pizotifen was observed on the
207 primary tumor. After 70 days from inoculation, bioluminescence imaging detected light
208 emitted in the lungs, livers and lymph nodes of vehicle-treated mice but not those of
209 Pizotifen-treated mice (Figure 3C). Vehicle-treated mice formed 5 to 50 metastatic

210 nodules per lung in all 10 mice analyzed; conversely, Pizotifen-treated mice (n=10)
211 formed 0 to 5 nodules per lung in all 10 mice analyzed (Figure 3D). Histological analyses
212 confirmed that metastatic lesions in the lungs were detected in all vehicle-treated mice;
213 conversely, they were detected in only 2 of 10 Pizotifen-treated mice and the rest of the
214 mice showed metastatic colony formations around the bronchiole of the lung. In addition,
215 4 of 10 vehicle-treated mice exhibited metastasis in the liver and the rest showed
216 metastatic colony formation around the portal tract of the liver. In contrast, none of 10
217 Pizotifen-treated mice showed liver metastases and only half of the 10 mice showed
218 metastatic colony formation around the portal tract (Figure 3E). These results indicate that
219 Pizotifen can suppress metastasis progression without affecting primary tumor growth.
220 To eliminate the possibility that the metastasis suppressing effects of Pizotifen
221 might result from off-target effects, we conducted validation experiments to determine
222 whether knockdown of HTR2C would show the same effects. The basic experimental
223 process followed the experimental design described above except that sub-clones of 4T1
224 cells that expressed shRNA targeting either LacZ or HTR2C were injected into the MFP
225 of female BALB/c mice and the mice were maintained without drug. Histological
226 analyses revealed that all of the mice (n=5) that were inoculated with 4T1 cells expressing
227 shRNA targeting LacZ showed metastases in the lungs. The mean number of metastatic
228 lesions in a lung was 26.4±7.8. In contrast, only one of the mice (n=5) were inoculated
229 with 4T1 cells expressing shRNA targeting HTR2C showed metastases in the lungs and
230 the rest of the mice showed metastatic colony formation around the bronchiole of the
231 lung. The mean number of metastatic lesions in the lung significantly decreased to 10% of
232 those of mice that were inoculated with 4T1 cells expressing shRNA targeting LacZ
233 (Figure 3F-H).
234 Taken together, pharmacological and genetic inhibition of HTR2C showed an
235 anti-metastatic effect in the 4T1 model system.
236

237 **HTR2C promoted EMT-mediated metastatic dissemination of human cancer cells**

238 Although pharmacological and genetic inhibition of HTR2C inhibited metastasis
239 progression, a role for HTR2C on metastatic progression has not been reported.
240 Therefore, we examined whether HTR2C could confer metastatic properties on poorly
241 metastatic cells.

242 Firstly, we established a stable sub-clone of MCF7 human breast cancer cells
243 expressing either vector control or HTR2C. Vector control expressing MCF7 cells
244 maintained highly organized cell-cell adhesion and cell polarity; however, HTR2C-
245 expressing MCF7 cells led to loss of cell-cell contact and cell scattering. The cobblestone-
246 like appearance of these cells was replaced by a spindle-like, fibroblastic morphology.
247 Western blotting and immunofluorescence (IF) analyses revealed that HTR2C-expressing
248 MCF7 cells showed loss of E-cadherin and EpCAM, and elevated expressions of N-
249 cadherin, vimentin and an EMT-inducible transcriptional factor Zeb1. Similar effects
250 were validated through another experiment using an immortal keratinocyte cell line,
251 HaCaT cells, in that HTR2C-expressing HaCaT cells also showed loss of cell-cell contact
252 and cell scattering with loss of epithelial markers and gain of mesenchymal markers
253 (Figure 4A-C). Therefore, both the morphological and molecular changes in the HTR2C-
254 expressing MCF7 and HaCaT cells demonstrated that these cells had undergone an EMT.

255 Next, we examined whether HTR2C-driven EMT could promote metastatic
256 dissemination of human cancer cells. Boyden chamber assay revealed that HTR2C
257 expressing MCF7 cells showed an increased cell motility and invasion compared with
258 vector control-expressing MCF7 cells in vitro (Figure 4D). Moreover, we conducted in
259 vivo examination of whether HTR2C expression could promote metastatic dissemination
260 of human cancer cells in a zebrafish xenotransplantation model. Red fluorescence protein-
261 labelled MCF7 cells expressing either vector control or HTR2C were injected into the
262 duct of Cuvier of *Tg* (*kdrl:eGFP*) zebrafish at 2 dpf. Twenty-four hours post injection, the
263 frequencies of the fish showing metastatic dissemination of the inoculated cells were

264 measured using fluorescence microscopy. In the fish that were inoculated with HTR2C
265 expressing MCF7 cells, the frequencies of the fish showing head, trunk, and end-tail
266 dissemination significantly increased to 96.7±4.7%, 68.8±6.4%, or 89.5±3.4%;
267 conversely, the frequency of the fish not showing any dissemination decreased to 0%
268 when compared with those in the fish that were inoculated with vector control expressing
269 MCF7 cells; 33.1±18.5%, 0%, 56.9± 4.4%, or 43% (Figure 4E and Table S6).
270 These results indicated that HTR2C promoted metastatic dissemination of cancer
271 cells though induction of EMT, and suggest that the screen can easily be converted to a
272 chemical genetic screening platform.
273
274 **Pizotifen induced mesenchymal to epithelial transition through inhibition of Wnt-**
275 **signaling.**
276 Finally, we elucidated the mechanism of action of how Pizotifen suppressed metastasis,
277 especially metastatic dissemination of cancer cells. Our results showed that HTR2C
278 induced EMT and that pharmacological and genetic inhibition of HTR2C suppressed
279 metastatic dissemination of MDA-MB-231 cells that had already transitioned to
280 mesenchymal-like traits via EMT. Therefore, we speculated that blocking HTR2C with
281 Pizotifen might inhibit the molecular mechanisms which follow EMT induction. We
282 firstly investigated the expressions of epithelial and mesenchymal markers in Pizotifen-
283 treated MDA-MB-231 cells since the activation of an EMT program needs to be transient
284 and reversible, and transition from a fully mesenchymal phenotype to a epithelial-
285 mesenchymal hybrid state or a fully epithelial phenotype is associated with malignant
286 phenotypes (22). IF and FACS analyses revealed 20% of Pizotifen-treated MDA-MB-231
287 cells restored E-cadherin expression. Also, western blotting analysis demonstrated that
288 4T1 primary tumors from Pizotifen-treated mice has elevated E-cadherin expression
289 compared with tumors from vehicle-treated mice (Figure 5A-C). However, mesenchymal
290 markers did not change between vehicle and Pizotifen-treated MDA-MB-231 cells (data

291 not shown). We further analyzed E-cadherin positive (E-cad$^+$) cells in Pizotifen-treated
292 MDA-MB-231 cells. The E-cad$^+$ cells showed elevated expressions of epithelial markers
293 KRT14 and KRT19; and decreased expression of mesenchymal makers vimentin, MMP1,
294 MMP3, and S100A4. Recent research reports that an EMT program needs to be transient
295 and reversible and that a mesenchymal phenotype in cancer cells is achieved by
296 constitutive ectopic expression of Zeb1. In accordance with the research, the E-cad$^+$ cells
297 and 4T1 primary tumors from Pizotifen-treated mice had decreased Zeb1 expression
298 compared with vehicle-treated cells and tumors from vehicle-treated mice (Figure 5D). In
299 contrast, HTR2C-expressing MCF7 and HuMEC cells expressed Zeb1 but not vehicle
300 control MCF7 and HuMEC cells (Figure 4C). These results indicate that HTR2C-
301 mediated signaling induced EMT through up-regulation of Zeb1 and blocking HTR2C
302 with Pizotifen induced mesenchymal to epithelial transition through downregulation of
303 Zeb1.

304 We further investigated the mechanism of action of how blocking HTR2C with
305 Pizotifen induced down-regulation of Zeb1. In embryogenesis, serotonin-mediated
306 signaling is required for Wnt-dependent specification of the superficial mesoderm during
307 gastrulation (23). In cancer cells, overexpression of HTR1D is associated with Wnt-
308 signaling which enables induction of EMT (24, 25). This evidence led to a hypothesis that
309 HTR2C-mediated signaling might turn on transcriptional activity of β-catenin and that
310 might induce up-regulation of EMT-TFs. IF analyses revealed β-catenin was accumulated
311 in the nucleus of HTR2C-expressing MCF7 cells but it was located in the cytoplasm of
312 vector control-expressing cells (Figure 5E). Nuclear accumulation of β-catenin in
313 HTR2C-expressing MCF7 cells was confirmed by western blot (Figure 5F). In contrast,
314 Pizotifen-treated MDA-MB-231 cells showed β-catenin located in the cytoplasm of the
315 cells. Vehicle-treated cells showed β-catenin accumulated in the nucleus of the cells.
316 (Figure 5G), and western blotting analysis confirmed that it was located in the cytoplasm
317 of Pizotifen-treated MDA-MB-231 cells (Figure 5H). Furthermore,

318 immunohistochemistry and western blotting analyses showed that β-catenin accumulated
319 in the nucleus, and phospho-GSKβ and Zeb1 expression were decreased in 4T1 primary
320 tumors from Pizotifen-treated mice compared with vehicle-treated mice (Figure 5C).
321 These results indicated that HTR2C would regulate transcriptional activity of β-catenin
322 and Pizotifen could inhibit it.
323 Taken together, we conclude that blocking HTR2C with Pizotifen restored
324 epithelial properties to metastatic cells (MDA-MB-231 and 4T1 cells) through a decrease
325 of transcriptional activity of β-catenin and that suppressed metastatic progression of the
326 cells.
327

328 **Figures and figure legends**

329 **Figure 1**

330

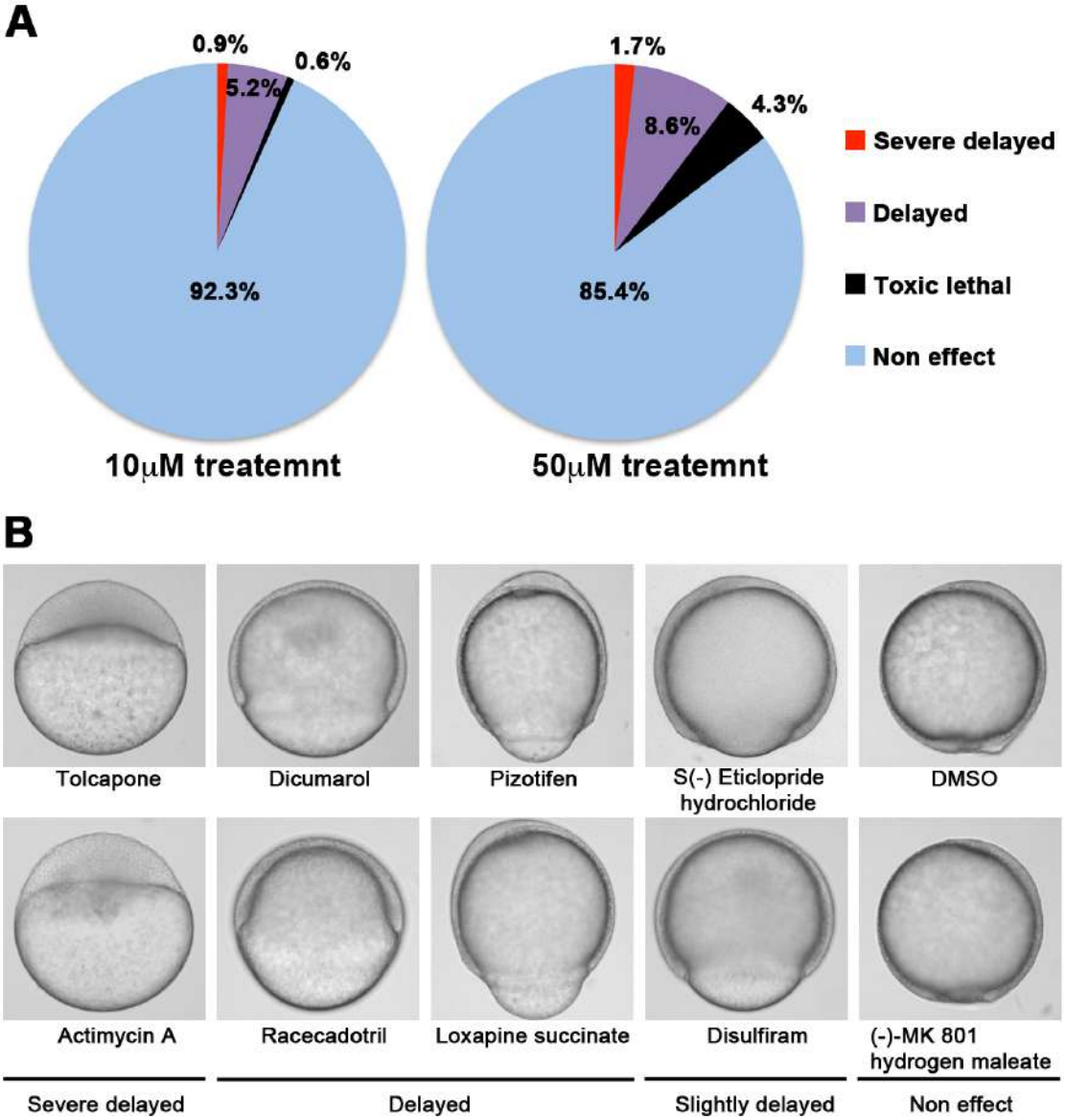

331

332

333 **Figure 1. A chemical screen for identification of epiboly-interrupting drugs.**

334 (A) Cumulative results of the chemical screen in which each drug was used at either

335 10μM (left) or 50μM (right) concentrations. 1,280 FDA, EMA or other agencies-

336 approved drugs were subjected to this screening. Positive "hit" drugs were those that

337 interrupted epiboly progression. (B) Representative samples of the embryos that were

338 treated with indicated drugs.

339 **Figure 2**

340

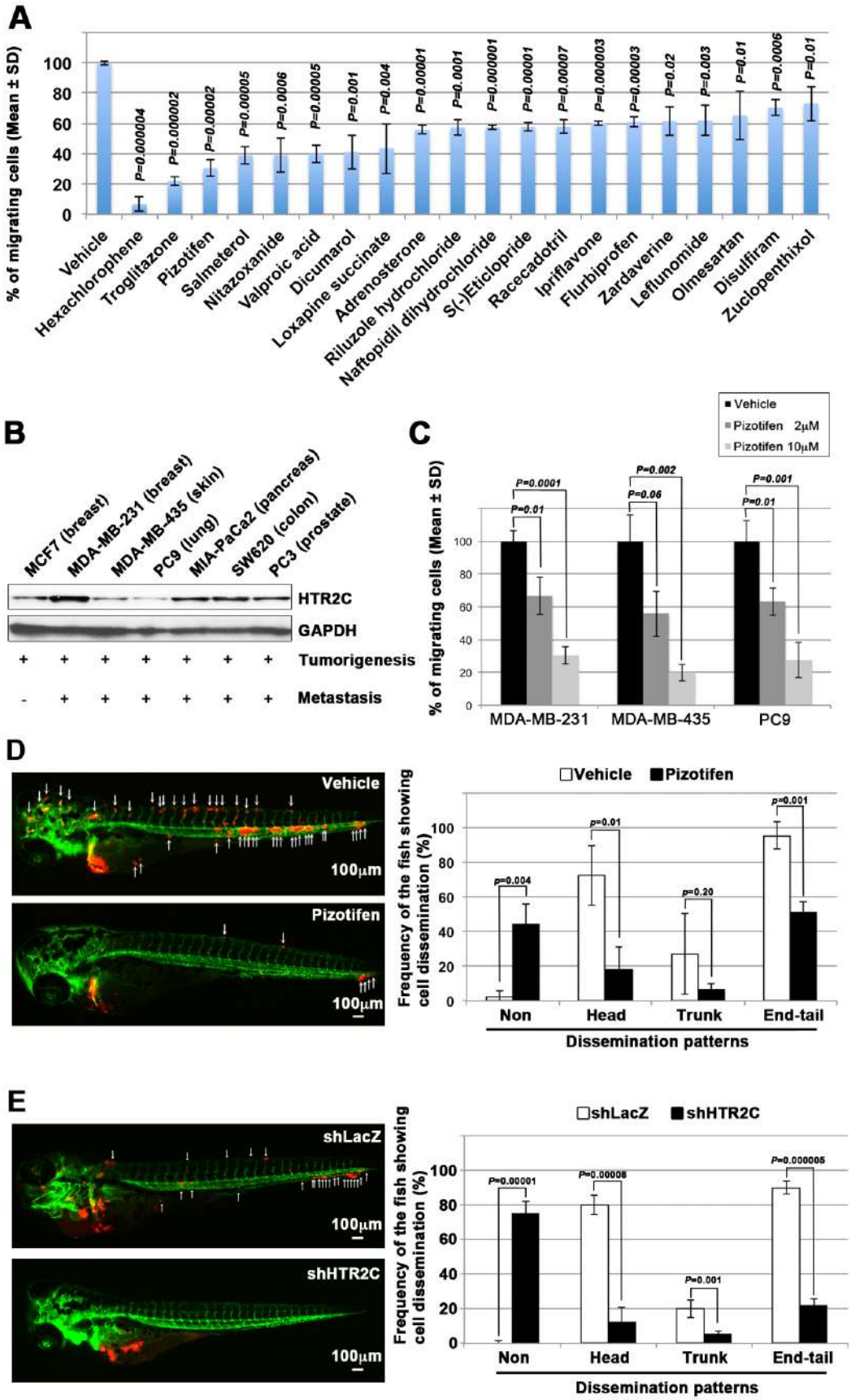

341

342 **Figure 2. Pizotifen, one of epiboly-interrupting drugs suppressed metastatic**

343 **dissemination of human cancer cells lines in vivo and vitro.**

344 (A) Effect of the epiboly-interrupting drugs on cell motility and invasion of MBA-MB-
345 231 cells. MBA-MB-231 cells were treated with vehicle or each of the epiboly-
346 interrupting drugs and then subjected to Boyden chamber assays. Fetal bovine serum
347 (1%v/v) was used as the chemoattractant in both assays. Each experiment was performed
348 at least twice. (B) Western blot analysis of HTR2C levels (top) in a non-metastatic human
349 cancer cell line, MCF7 (breast) and highly metastatic human cancer cell lines, MDA-MB-
350 231 (breast), MDA-MB-435 (melanoma), PC9 (lung), MIA-PaCa2 (pancreas), PC3
351 (prostate) and SW620 (colon); GAPDH loading control is shown (bottom). (C) Effect of
352 pizotifen on cell motility and invasion of MBA-MB-231, MDA-MB-435 and PC9 cells.
353 Either vehicle or pizotifen treated the cells were subjected to Boyden chamber assays.
354 Fetal bovine serum (1%v/v) was used as the chemoattractant in both assays. Each
355 experiment was performed at least twice. (D) and (E) Representative images of
356 dissemination of 231R, shLacZ 231R or shHTR2C 231R cells in zebrafish
357 xenotransplantation model. The fish larvae that were inoculated with 231R cells, were
358 treated with either vehicle (top left) or the drug (lower left) (D). The fish larvae that were
359 inoculated with either shLacZ 231R or shHTR2C 231R cells (lower left) (E). White
360 arrows head indicate disseminated 231R cells. The images were shown in 4x
361 magnification. Scale bar, 100μm. The mean frequencies of the fish showing head, trunk,
362 or end-tail dissemination were counted (graph on right). Each value is indicated as the
363 mean ± SEM of two independent experiments. Statistical analysis was determined by
364 Student's t test. See also Figure S2 and S3, Table S3-S5.
365

366 **Figure 3**

367

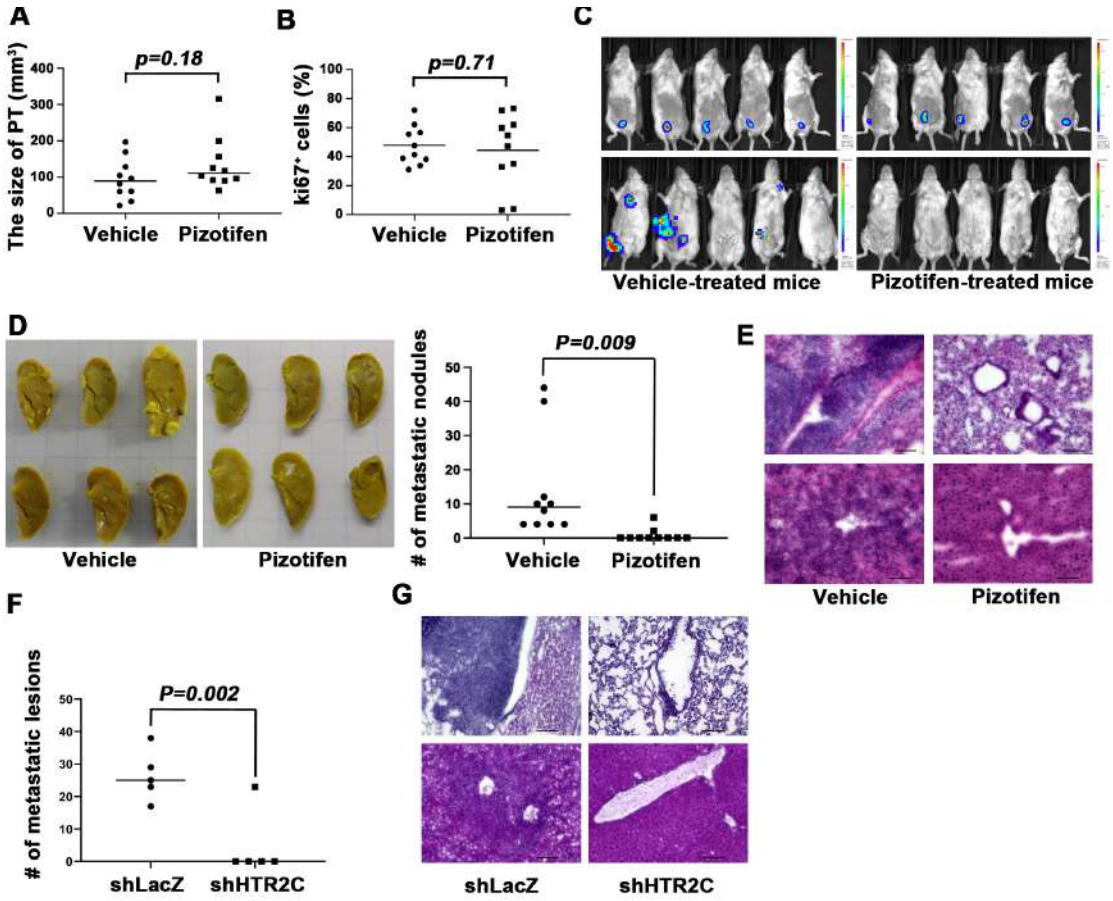

368

369

370 **Figure 3. Pizotifen suppressed metastatic progression in a mouse model of**

371 **metastasis.**

372 (A) Mean volumes (n=10 per group) of 4T1 primary tumors formed in the mammary fat

373 pad of either vehicle or Pizotifen-treated mice at day 10 post injection. (B) Ki67

374 expression level in 4T1 primary tumors formed in the mammary fat pad of either vehicle

375 or Pizotifen-treated mice at day 10 post injection. The mean expression levels of Ki67

376 (n=10 mice per group) were determined and were calculated as the mean ration of Ki67

377 positive cells to DAPI area. (C) Representative images of primary tumors on day 10 post

378 injection (top panels) and metastatic burden on day 70 post injection (bottom panels)

379 taken using an IVIS Imaging System. (D) Representative images of the lungs from either

380 vehicle (top) or Pizotifen-treated mice (bottom) at 70 days past tumor inoculation.

381 Number of metastatic nodules in the lung of either vehicle or Pizotifen-treated mice
382 (right). (E) Representative H&E staining of the lung (top) and liver (bottom) from either
383 vehicle or Pizotifen-treated mice. (F) The mean number of metastatic lesions in step
384 sections of the lungs from the mice that were inoculated with 4T1-12B cells expressing
385 shRNA targeting for either LacZ or HTR2C. (G) Representative H&E staining of the lung
386 and liver from the mice that were inoculated with 4T1-12B cells expressing shRNA
387 targeting for either LacZ or HTR2C. Each value is indicated as the mean ± SEM.
388 Statistical analysis was determined by Student's *t* test.
389

390 **Figure 4**

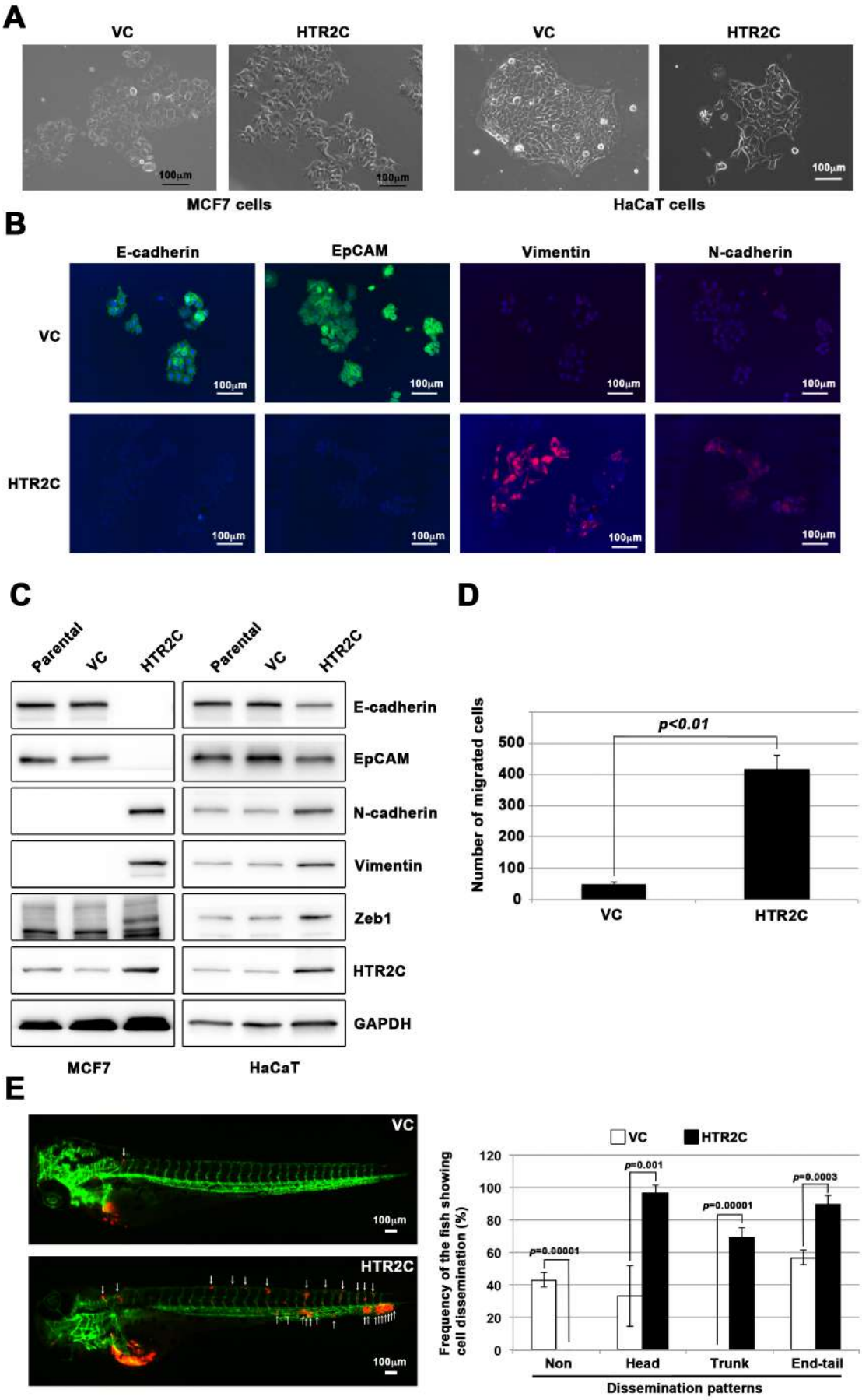

391

392 **Figure 4. HTR2C induced EMT-mediated metastatic dissemination of human cancer**
393 **cells.**
394 (A) The morphologies of the MCF7 and HaCaT cells expressing either the control vector
395 or HTR2C were revealed by phase contrast microscopy. (B) Immunofluorescence staining
396 of E-cadherin, EpCAM, Vimentin, and N-cadherin expressions in the MCF7 cells from
397 Figure 4A. (C) Expression of E-cadherin, EpCAM, Vimentin, N-cadherin, and HTR2C
398 was examined by western-blotting in the MCF7 and HaCaT cells; GAPDH loading
399 control is shown (bottom). (D) Effect of HTR2C on cell motility and invasion of MCF7
400 cells. MCF7 cells were subjected to Boyden chamber assays. Fetal bovine serum (1%v/v)
401 was used as the chemoattractant in both assays. Each experiment was performed at least
402 twice. (E) Representative images of dissemination patterns of MCF7 cells expressing
403 either the control vector (top left) or HTR2C (lower left) in a zebrafish
404 xenotransplantation model. White arrows head indicate disseminated MCF7 cells. The
405 mean frequencies of the fish showing head, trunk, or end-tail dissemination tabulated
406 (right). Each value is indicated as the mean ± SEM of two independent experiments.
407 Statistical analysis was determined by Student's *t* test.
408 See also Table S6.

409 **Figure 5**

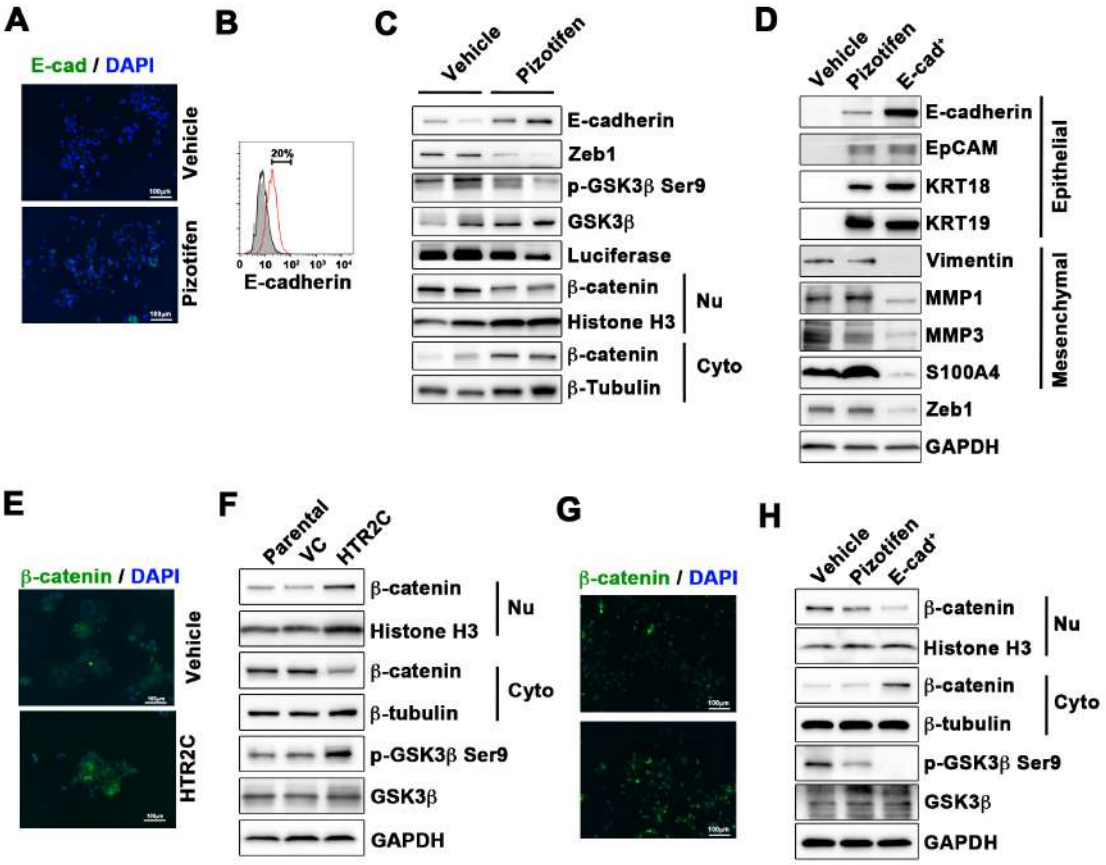

410

411 **Figure 5. Pizotifen restored mesenchymal-like traits of MDA-MB-231 cells into**

412 **epithelial traits through blocking nuclear accumulation of β-catenin.**

413 (A) IF staining of E-cadherin in either vehicle or Pizotifen-treated MDA-MB-231 cells.

414 (B) Surface expression of E-cadherin in either vehicle (black) or Pizotifen (red)-treated

415 MDA-MB-231 cells by FACS analysis. Non-stained controls are shown in gray. (C)

416 Protein expressions levels of E-cadherin, Zeb1, and β-catenin in the cytoplasm and

417 nucleus of 4T1 primary tumors from either vehicle or Pizotifen-treated mice are shown;

418 Luciferase, Histone H3, and β-tubulin are used as loading control for whole cell, nuclear

419 or cytoplasmic lysate, respectively. (D) Protein expression levels of epithelial and

420 mesenchymal markers and Zeb1 in either vehicle or Pizotifen-treated MDA-MB-231 cells

421 or E-cadherin positive (E-cad^{+}) cells in Pizotifen-treated MDA-MB-231 cells are shown.

422 (E) Immunofluorescence staining of β-catenin in the MCF7 cells expressing either vector

423 control or HTR2C. (F) Expressions of β-catenin in the cytoplasm and nucleus of MCF7

424 cells. (G) IF staining of β-catenin in either vehicle or Pizotifen-treated MDA-MB-231

425 cells. (H) Expressions of β-catenin in the cytoplasm and nucleus of MDA-MB-231 cells

426 and the E-cad^{+} cells.

427

428 **Table 1. Primary targets of the identified drugs**

429

The identified drugs	Primary targets of the identified drugs
Hexachlorophene	D-lactate dehydrogenase (D-LDH), not expressed in mammalian cells
Troglitazone	Agonist for Peroxisome proliferator-activated receptor α and γ (PPARα and γ)
Pizotifen malate	5-hydroxytryptamine receptor 2C (HTR2C)
Salmeterol	Adrenergic receptor beta 2 (ADRB2)
Nitazoxanide	Pyruvate ferredoxin oxidoreductase (PFOR), not expressed in mammalian cells
Valproic acid	Histone deacetylases (HDACs)
Dicumarol	NAD(P)H dehydrogenase quinone 1 (NQO1)
Loxapine succinate	Dopamine receptor D2 and D4 (DRD2 and DRD4)
Adrenosterone	Hydroxysteroid (11-beta) dehydrogenase 1 (HSD11β1)
Riluzole hydrochloride	Glutamate R and Voltage-dependent Na+ channel
Naftopidil dihydrochloride	5-hydroxytryptamine receptor 1A (HTR1A) and α1-adrenergic receptor (AR)
S(-)Eticlopride hydrochloride	Dopamine receptor D2 (DRD2)
Racecadotril	Membrane metallo-endopeptidase (MME)
Ipriflavone	Unknow
Flurbiprofen	Cyclooxygenase 1 and 2 (Cox1 and 2)
Zardaverine	Phosphodiesterase III/IV (PDE3/4)
Leflunomide	Dihydroorotate dehydrogenase (DHODH)
Olmesartan	Angiotensin II receptor alpha
Disulfiram	Aldehyde dehydrogenase (ALDH) Dopamine β-hydroxylase (DBH)
Zuclopenthixol dihydrochloride	Dopamine receptors D1 and D2 (DRD1 and 2)

430

431 **Discussion**

432 Reducing or eliminating mortality associated with metastatic disease is a key goal of
433 medical oncology, but few models exist that allow for rapid, effective screening of novel
434 compounds that target the metastatic dissemination of cancer cells. Based on accumulated

435 evidence that at least fifty genes play an essential role in governing both metastasis and
436 gastrulation progression (Table 1S), we hypothesized that small molecule inhibitors that
437 interrupt gastrulation of zebrafish embryos might suppress metastatic progression of
438 human cancer cells. We created a unique screening concept utilizing gastrulation of
439 zebrafish embryos to test the hypothesis. Our results clearly confirmed our hypothesis:
440 25.6% (20/76 drugs) of epiboly-interrupting drugs could also suppress cell motility and
441 invasion of highly metastatic human cell lines in vitro. In particular, Pizotifen which is an
442 antagonist for serotonin receptor 2C and one of the epiboly-interrupting drugs, could
443 suppress metastasis in a mouse model (Figure 3A-E). Thus, this screen could offer a novel
444 platform for discovery of anti-metastasis drugs.
445 There are at least two advantages to the screen described herein. One is that the
446 screen can easily be converted to a chemical genetic screening platform. Indeed, we have
447 provided the first evidence that HTR2C, which is a primary target of Pizotifen, induced
448 EMT and promoted metastatic dissemination of cancer cells (Figure 4A-E). In this
449 research, 1,280 FDA approval drugs were screened, this is less than a few percent of all of
450 druggable targets (approximately 100 targets) in the human proteome in the body. If
451 chemical genetic screening using specific inhibitor libraries were conducted, more genes
452 that contribute to metastasis and gastrulation could be identified. The second advantage is
453 that the screen enables one researcher to test 100 drugs in 5 hours with using optical
454 microscopy, drugs, and zebrafish embryos. That indicates this screen is not only highly
455 efficient, low-cost, and low-labor but also enables researchers who do not have high
456 throughput screening instruments to conduct drug screening for anti-metastasis drugs.
457

458 **Acknowledgments**

459 We sincerely appreciate Dr. Joshua Collins (NIH/NIDCR) and Dr. Diane Palmieri
460 (NIH/NCI) for helping this research. We thank Dr. Herrick (Albany medical collage) for
461 providing pCMV-h5TH2C-VSV with us. This study was funded by grants from National

Medical Research Council of Singapore (R-154000547511) and Ministry of Education of Singapore (R-154000A23112) to Z.G.

Author Contributions

Design research; J.N. Conducting experiments; J.N. and L.T. Analyzing data: J.N. Writing the paper; J.N. and Z.G. Funding Acquisition; Z.G, S.W. B.C.G., H.M. and Supervision; Z.G.

Declaration of Interests

J.N., L.T., B.C.G., S.W., H.M. and G.Z. declare no conflict of interest.

Materials and Methods

Zebrafish embryo screening

Zebrafish embryos at two cell stage were collected at 20 mins after their fertilization. Each drug was added to a well of a 24-well plate containing approximately 20 zebrafish embryos per well in either 10 μM or 50 μM final concentration when the embryos reached the sphere stage. Chemical treatment was initiated at 4 hours post-fertilization (hpf) and approximately 20 embryos were treated with two different concentrations for each compound tested. The treatment was ended at 9 hpf when vehicle (DMSO) treated embryos as control reach 80-90% completion of the epiboly stage. The compounds which induced delay (<50% epiboly) in epiboly were selected as hit compounds for in vitro testing using highly metastatic human cancer cell lines. The study protocol was approved by the Institutional Animal Care and Use Committee of the National University of Singapore (protocol number: R16-1068).

Reagents

488 FDA, EMA and other agencies approved chemical libraries was purchased from
489 Prestwick Chemical (Illkirch, France). Pizotifen and S(-) Eticlopride hydrochloride were
490 purchased from Sigma-Aldrich (St. Louis, MO).
491
492 **Cell culture and cell viability assay**
493 MCF7, MDA-MB-231, MDA-MB-435, MIA-PaCa2, PC3, SW620, PC9 and HaCaT cells
494 were obtained from American Type Culture Collection (ATCC, Manassas, VA).
495 Luciferase-expressing 4T1 (4T1-12B) cells were provided from Dr. Gary Sahagian (Tufts
496 University, Boston, MA). All culture methods followed the supplier's instruction. Cell
497 viability assay was performed as previously described (16).
498
499 **Plasmid**
500 A DNA fragment coding for HTR2C was amplified by PCR with primers containing
501 restriction enzyme recognition sequences. The HTR2C coding fragment was amplified
502 from hsp70l:mCherry-T2A-CreERT2 plasmid (17).
503
504 **Immunoblotting**
505 Western blotting was performed as described previously (16). Anti-PRMT1, anti-
506 CYP11A1, anti-E-cadherin, anti-EpCAM, anti-Vimentin, anti-N-cadherin, anti-Zeb1,
507 anti-Histone H_3, anti-α-tubulin and anti-GAPDH antibodies were purchased from Cell
508 signaling Technology. Anti-HTR2C and anti-DRD2 antibodies were purchased form
509 Abcam. Anti-phospho-GSK3β (Ser9), anti-GSK3β, Anti-KRT18, anti-KRT19, anti-
510 MMP1, anti-MMP2, anti-S100A4, anti-Luciferase, and anti-β-catenin antibodies were
511 purchased from Santa Cruz.
512
513 **Flow cytometry**

514 Cells were stained with FITC-conjugated E-cadherin antibody (Biolegend, San Diego,
515 CA). Flow cytometry was performed as described (26) and analyzed with FlowJo
516 software (TreeStar, Ashland, OR).
517
518 **shRNA mediated gene knockdown**
519 The short hairpin RNA (shRNA)-expressing lentivirus vectors were
520 constructed using pLVX-shRNA1 vector (Clontech). PRMT1-shRNA_#3–targeting
521 sequence is GTGTTCCAGTATCTCTGATTA; PRMT1-shRNA_#4–targeting sequence
522 is TTGACTCCTACGCACACTTTG. CYP11A1-shRNA_#4–targeting sequence is
523 GCGATTCATTGATGCCATCTA; CYP11A1-shRNA_#4–targeting sequence is
524 GAAATCCAACACCTCAGCGAT. Human HTR2C-shRNA–targeting sequence is
525 TCATGCACCTCTGCGCTATAT. Mouse HTR2C-shRNA–targeting sequence is
526 CTTCATACCGCTGACGATTAT. LacZ-shRNA– targeting sequence is
527 CTACACAAATCAGCGATT.
528
529 **Immunofluorescence**
530 Immunofluorescence microscopy assay was performed by previously described (16). Goat
531 anti-mouse and goat anti-rabbit immunoglobulin G (IgG) antibodies conjugated to Alexa
532 Fluor 488 (Life Technologies) and diluted at 1:100 were used. Nuclei were visualized by
533 the addition of 2μg/ml of 4', 6-diamidino-2-phenylindole (DAPI) and photographed at
534 100x magnification by a fluorescent microscope BZ-X700 (KEYENCE, Japan).
535
536 **Boyden chamber cell motility and invasion assay**
537 These assays were performed by previously described (16). In Boyden chamber assay,
538 either $3x10^5$ MDA-MB-231, $1x10^6$ MDA-MB-435, or $5x10^5$ PC9 cells were applied to
539 each well in the upper chamber.
540

541 **Zebrafish xenotransplantation model**

542 *Tg(kdrl:eGFP)* zebrafish was provided by Dr. Stainier (Max Planck Institute for Heart and
543 Lung Research). Embryos that were derived from the line were maintained in E3 medium
544 containing 200μM 1-phenyl-2-thiourea (PTU). Approximately 100-400 Red fluorescence
545 protein (RFP)-labelled MBA-MB-231 or MIA-Paca2 cells were injected into the duct of
546 Cuvier of the zebrafish at 2dpf. The fish were randomly assigned to two groups. One group
547 was maintained in the presence of pizotifen-containing E3 medium and the other group was
548 maintained in vehicle-containing E3 medium.

549

550 **Spontaneous metastasis mouse model**

551 4T1-12B cells ($2x10^4$) were injected into the #4 mammary fat pad while the mice were
552 anesthetized. To monitor tumor growth and metastases, mice were imaged biweekly by
553 IVIS Imaging System (ParkinElmer). The primary tumor was resected 10 days after
554 inoculation. The study protocol (protocol number: BRC IACUC #110612) was approved
555 by A*STAR (Agency for Science, Technology and Research, Singapore).

556

557 **Histological Analysis**

558 All OCT embedded primary tumors, lungs, and livers of mice from the spontaneous
559 metastasis 4T1 model were sectioned on a cryostat. Eight micron sections were taken at
560 five hundred micron intervals through the entirety of the livers and lungs. Sections were
561 subsequently stained with hematoxylin and eosin. Metastatic lesions were counted under a
562 microscope in each section for both lungs and livers.

563

564 **Statistics**

565 Data were analyzed by Student's t test; $p < 0.05$ was considered significant.

566

567 **References**

568 1. Chambers AF, Groom AC, & MacDonald IC (2002) Dissemination and growth
569 of cancer cells in metastatic sites. *Nature reviews. Cancer* 2(8):563-572.
570 2. Steeg PS (2003) Metastasis suppressors alter the signal transduction of
571 cancer cells. *Nature reviews. Cancer* 3(1):55-63.
572 3. Fidler IJ (2003) The pathogenesis of cancer metastasis: the 'seed and soil'
573 hypothesis revisited. *Nature reviews. Cancer* 3(6):453-458.
574 4. Cavallaro U & Christofori G (2004) Cell adhesion and signalling by cadherins
575 and Ig-CAMs in cancer. *Nature reviews. Cancer* 4(2):118-132.
576 5. Ellenbroek SI, Iden S, & Collard JG (2012) Cell polarity proteins and cancer.
577 *Semin Cancer Biol* 22(3):208-215.
578 6. Tsai JH & Yang J (2013) Epithelial-mesenchymal plasticity in carcinoma
579 metastasis. *Genes & development* 27(20):2192-2206.
580 7. Solnica-Krezel L (2005) Conserved patterns of cell movements during
581 vertebrate gastrulation. *Curr Biol* 15(6):R213-228.
582 8. Latimer A & Jessen JR (2010) Extracellular matrix assembly and organization
583 during zebrafish gastrulation. *Matrix Biol* 29(2):89-96.
584 9. Solnica-Krezel L (2006) Gastrulation in zebrafish -- all just about adhesion?
585 *Curr Opin Genet Dev* 16(4):433-441.
586 10. Tsai YJ*, et al.* (2011) The predominant protein arginine methyltransferase
587 PRMT1 is critical for zebrafish convergence and extension during
588 gastrulation. *FEBS J* 278(6):905-917.
589 11. Hsu HJ, Liang MR, Chen CT, & Chung BC (2006) Pregnenolone stabilizes
590 microtubules and promotes zebrafish embryonic cell movement. *Nature*
591 439(7075):480-483.
592 12. Weinbach EC & Garbus J (1969) Mechanism of Action of Reagents that
593 uncouple Oxidative Phosphorylation. *Nature* 221:1016.
594 13. Sack U*, et al.* (2011) Novel effect of antihelminthic Niclosamide on S100A4-
595 mediated metastatic progression in colon cancer. *Journal of the National*
596 *Cancer Institute* 103(13):1018-1036.
597 14. Huang EW*, et al.* (2012) Vinpocetine inhibits breast cancer cells growth in
598 vitro and in vivo. *Apoptosis : an international journal on programmed cell*
599 *death* 17(10):1120-1130.
600 15. Szilágyi G*, et al.* (2005) Effects of vinpocetine on the redistribution of cerebral
601 blood flow and glucose metabolism in chronic ischemic stroke patients: a PET
602 study. *Journal of the Neurological Sciences* 229-230:275-284.
603 16. Nakayama J, Lu J, Makinoshima H, & Gong Z (2020) A Novel Zebrafish Model
604 of Metastasis Identifies the HSD11β1 Inhibitor Adrenosterone as a
605 Suppressor of Epithelial-Mesenchymal Transition and Metastatic
606 Dissemination. *Mol Cancer Res* 18(3):477-487.
607 17. Kolosionek E*, et al.* (2009) Expression and activity of phosphodiesterase
608 isoforms during epithelial mesenchymal transition: the role of
609 phosphodiesterase 4. *Mol Biol Cell* 20(22):4751-4765.
610 18. Sasaki T*, et al.* (2014) Serum CD10 is associated with liver metastasis in
611 colorectal cancer. *J Surg Res.* 192(2):390-394.
612 19. Liu P*, et al.* (2013) Disulfiram targets cancer stem-like cells and reverses
613 resistance and cross-resistance in acquired paclitaxel-resistant triple-
614 negative breast cancer cells. *British journal of cancer* 109(7):1876-1885.
615 20. Gunnarsson L, Jauhiainen A, Kristiansson E, Nerman O, & Larsson DGJ (2008)
616 Evolutionary conservation of human drug targets in organisms used for
617 environmental risk assessments. *Environmental Science & Technology*
618 42(15):5807-5813.
619 21. Tao K, Fang M, Alroy J, & Sahagian GG (2008) Imagable 4T1 model for the
620 study of late stage breast cancer. *BMC cancer* 8:228.

621 22. Kröger C, Afeyan, A.; Mraz, J.; Eaton, EN.; Reinhardt, F.; Khodor, YL.; Thiru, P.;
622 Bierie B.; Ye, X.; Burge, CB.; Weinberg RA (2019) Acquisition of a hybrid E/M
623 state is essential for tumorigenicity of basal breast cancer cells. *Proceedings*
624 *of the National Academy of Sciences of the United States of America*
625 116(15):7353-7362.
626 23. Beyer TD, M.; Thumberger, T.; Vick, P.; Tisler, M.; Schneider, I.; Bogusch, S.;
627 Andre, P.; Ulmer, B.; Walentek, P.; Niesler, B.; Blum, M.; Schweickert, A.
628 (2012) Serotonin signaling is required for Wnt-dependent GRP specification
629 and leftward flow in Xenopus. *Curr Biol* 22(1):33-39.
630 24. Sui HX, H.; Ji, Q.; Liu, X.; Zhou, L.; Song, H.; Zhou, X.; Xu, Y.; Chen, Z.; Cai, J.; Ji, G.;
631 Li, Q. (2015) 5-hydroxytryptamine receptor (5-HT1DR) promotes colorectal
632 cancer metastasis by regulating Axin1/β-catenin/MMP-7 signaling pathway.
633 *Oncotarget* 6(28):25975-25987.
634 25. Zhan TR, N.; Boutros, M. (2017) Wnt signaling in cancer. *Oncogene*
635 36(11):1461–1473.
636 26. Nakayama J*, et al.* (2009) BLNK suppresses pre-B-cell leukemogenesis
637 through inhibition of JAK3. *Blood* 113(7):1483-1492.
638

639

640 **Supplemental Information**

641

642 **Figure S1.**

643

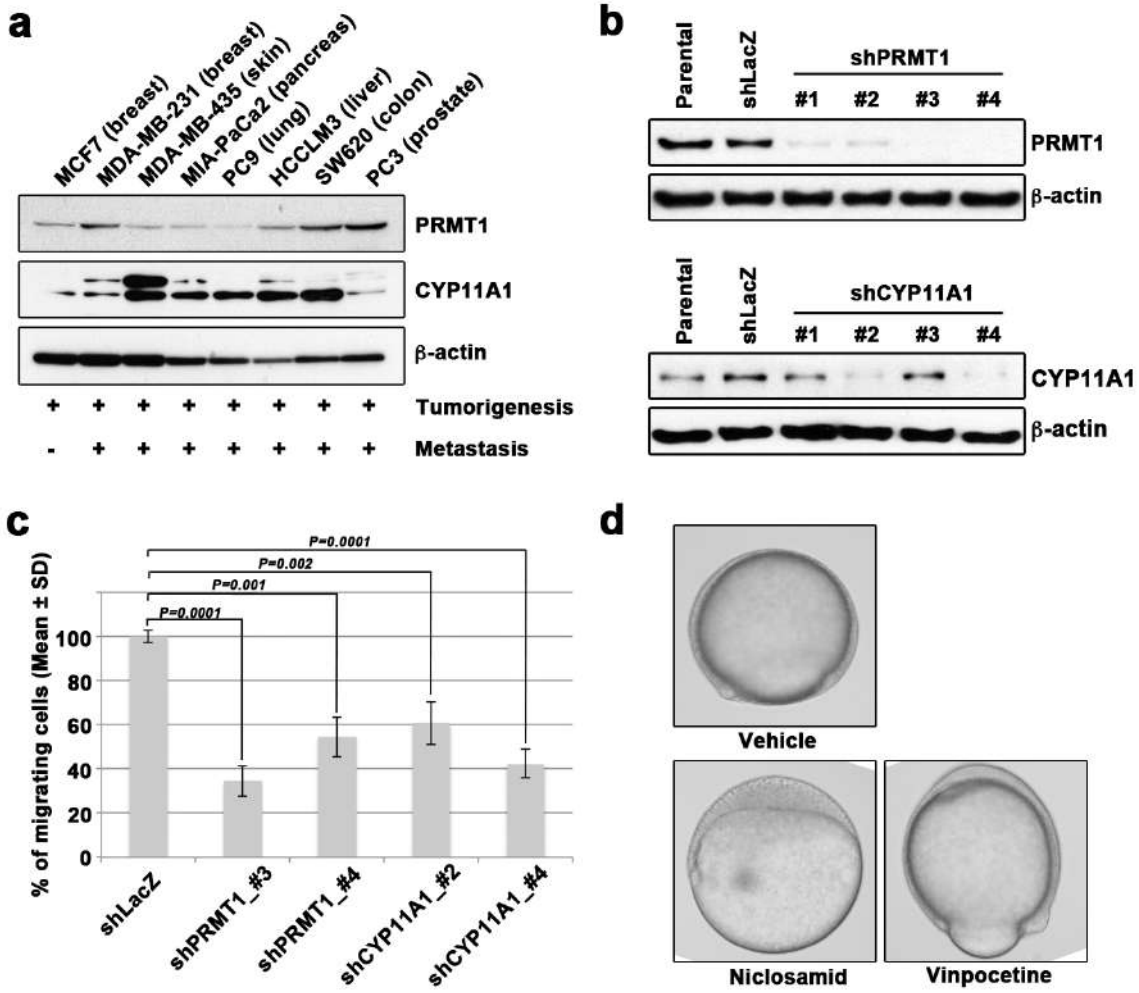

644

645

646 **Figure S1. Molecular mechanisms of epiboly in zebrafish overlap with those in**

647 **cancer metastasis.**

648 (A) Western blot analysis of PRMT1 (upper) and CYP11A1 (middle) protein levels in

649 non-metastatic human cancer cell line (MCF7) and highly metastatic human cancer cell

650 lines (MDA-MB-231, MDA-MB-435, MIA-PaCa2, PC9, HCCLM3, PC3 and SW620); β-

651 actin loading control is shown (bottom). (B) Knockdown of PRMT1 or CYP11A1 in

652 MDA-MB-231 cells. MBA-MB-231 cells were transfected with a control shRNA

653 targeting LacZ, and one of four independent shRNAs targeting PRMT1 (clone #1 to

654 #4) or one of two independent shRNAs targeting CYP11A1 (clone #1 to #4). Reduced

655 PRMT1 and CYP11A1 expression, determined by western blot, in sub-cell lines of

656 MDA-MB-231 cells expressing PRMT1 shRNA (clone #3 and #4 or CYP11A1 (clone
657 #2 and #4), compared with controls (parental cell line MDA-MB-231 and control
658 shRNA cells); β-actin levels shown as a loading control. (C) Effect of shRNAs
659 targeting either PRMT1 or CYP11A1 on cell motility and invasion of MBA-MB-231
660 cells. Parental MDA-MB-231 cells and four sub-cell lines of MDA-MB-231 cells that
661 were transfected with either shRNA targeting either LacZ, two independent shRNAs
662 targeting PRMT1 (clone #3 and #4) or two independent shRNAs targeting CYP11A1
663 (clone #2 and #4), were subjected to Boyden chamber assays. (D) Zebrafish embryos
664 treated with either vehicle (DMSO), 10μM Niclosamide, or 50μM vinpocetine.
665 Approximately 20 embryos were treated with either DMSO as a vehicle control,
666 niclosamide, or vinpocetine. The treatment was started at 4 hpf when all of embryos
667 reached sphere stage and ended at 9 hpf when control embryos reached 80-90%
668 epiboly stage. Each experiment was performed at least twice. Statistical analysis was
669 determined by Student's *t* test.
670

Figure S2.

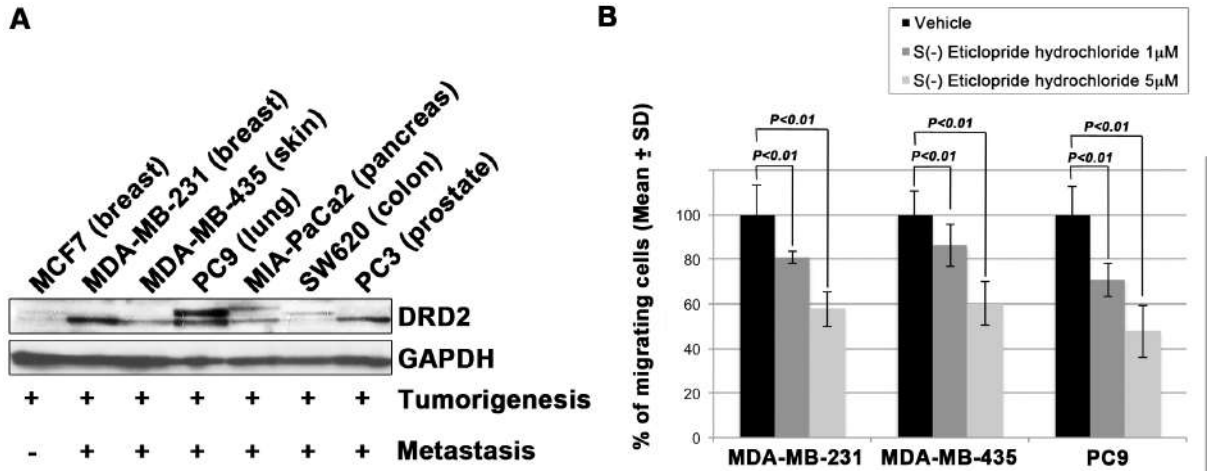

Figure S2. S (-) Eticlopride hydrochloride suppressed cell motility and invasion of human cancer cells.

Related to Figure 2.

(A) Western blot analysis of DRD2 levels in non-metastatic human cancer cell line, MCF7 (breast) and highly metastatic human cancer cell lines, MDA-MB-231 (breast), MDA-MB-435 (melanoma), MIA-PaCa2 (pancreas), PC3 (prostate) and SW620 (colon); GAPDH loading control is shown (bottom). (B) Effect of S (-) Eticlopride hydrochloride on cell motility and invasion of MBA-MB-231, MDA-MB-435, and PC9 cells. Either vehicle or pizotifen treated cells were subjected to Boyden chamber assays. Fetal bovine serum (1%v/v) was used as the chemoattractant in both assays. Each experiment was performed at least twice. Statistical analysis was determined by Student's *t* test.

688 **Figure S3.**

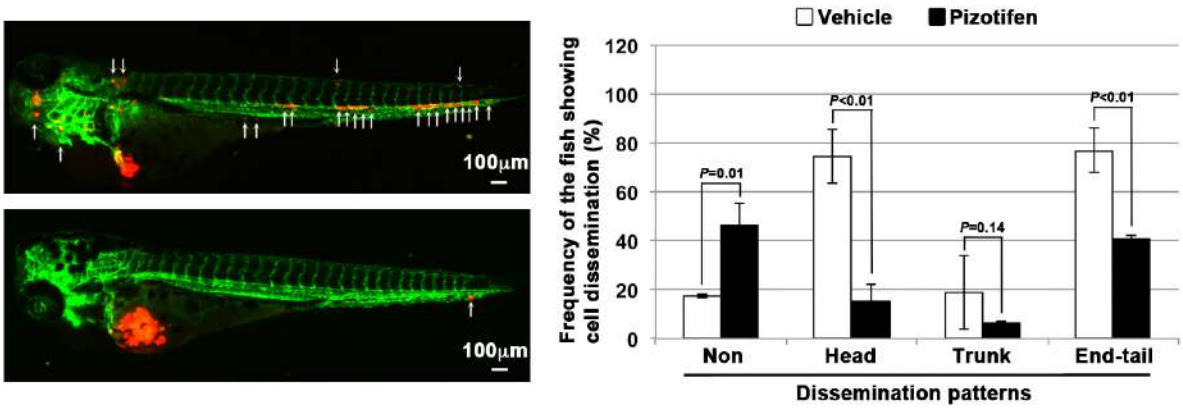

689

690 **Figure S3. Pizotifen suppressed metastatic dissemination of human pancreatic**

691 **cancer cells in a zebrafish xenotransplantation model.**

692 Related to Figure 2.

693 Representative images of dissemination of MIA-PaCa2 cells in zebrafish

694 xenotransplantation model. The fish were inoculated with MIA-PaCa2 cells, and treated

695 with either vehicle (top left) or drug (lower left). White arrows heads indicate

696 disseminated MIA-PaCa2 cells. The images were shown in 4x magnification. Scale bar,

697 100μm. The mean frequencies of the fish showing head, trunk, or end-tail dissemination

698 were tabulated (right). Each value is indicated as the mean ± SEM of two independent

699 experiments. Statistical analysis was determined by Student's *t* test.

700

701 **Table S1. A list of the genes that are involved between gastrulation and**
702 **metastasis progression**
703

Genes	Gastrulation Defects	Ref	Effects in Metastasis	Ref
BMP	Convergence and extension	(1)	EMT	(2)
WNT	Convergence and extension	(3)	Migration and Invasion	(4)
FGF	Convergence and extension	(5)	Invision	(6)
EGF	Epiboly	(7)	Migration	(8)
PDGF	Convergence and extension	(9)	EMT	(10)
CXCL12	Migration of endodermal cells	(11)	Migration and Invasion	(12)
CXCR4	Migration of endodermal cells	(11)	Migration and Invasion	(12)
PIK3CA	Convergence and extension	(13)	Migration and Invasion	(14)
YES	Epiboly	(15)	Migration	(16)
FYN	Epiboly	(17)	Migration and Invasion	(18)
MAPK1	Epiboly	(19)	Migration	(20)
SHP2	Convergence and extension	(21)	Migration	(22)
SNAI1	Convergence and extension	(23)	EMT	(24)
SNAI2	Mesoderm & Neural crest formation	(25)	EMT	(95)
TWIST1	Mesoderm formation	(26)	EMT	(27)
TBXT	Convergence and extension	(3)	EMT	(28)
ZEB1	Epiboly	(29)	EMT	(30)
GSC	Mesodermal patterning	(31)	EMT	(32)
FOXC2	Unclear, defects in gastrulation	(33)	EMT	(34)
STAT3	Convergence and extension	(35)	Migration	(36)
POU5F1	Epiboly	(37)	EMT	(38)
EZH2	Unclear, defects in gastrulation	(39)	Invasion	(40)
EHMT2	Defects in Neurogenesis	(41)	Migration and Invasion	(42)
BMI1	Defects in skelton formation	(43)	EMT	(44)
RHOA	Convergence and extension	(45)	Migration and Invasion	(46)
CDC42	Convergence and extension	(47)	Migration and Invasion	(48)
RAC1	Convergence and extension	(49)	Migration and Invasion	(50)
ROCK2	Convergence and extension	(51)	Migration and Invasion	(52)
PAR1	Convergence and extension	(53)	Migration	(54)
PRKCI	Convergence and extension	(53)	EMT	(55)
CAP1	Convergence and extension	(56)	Migration	(57)
EZR	Epiboly	(58)	Migration	(59)
EPCAM	Epiboly	(60)	Migration and Invasion	(61)
ITGB1 / ITA5	Mesodermal Migration	(62)	Migration and Invasion	(63)
FN1	Convergence and extension	(64)	Invasion	(65)
HAS2	Dorsal migration of lateral cells	(66)	Invasion	(67)
MMP14	Convergence and extension	(68)	Invasion	(69)
COX1	Epiboly	(70)	Invasion	(71)
PTGES	Convergence and extension	(72)	Invasion	(73)
SLC39A6	Aterior migration	(74)	EMT	(75)
GNA12 / 13	Convergence and extension	(41)	Migration and Invasion	(76)
OGT	Epiboly	(77)	Migration and Invasion	(78)
CCN1	Cell Movement	(79)	Migration and Invasion	(80)
TRPM7	Convergence and extension	(81)	Migration	(82)
MAPKAPK2	Epiboly	(83)	Migration	(84)
B4GALT1	Convergence and extension	(85)	Invasion	(86)
IER2	Convergence and extension	(87)	Migration	(88)
TIP1	Convergence and extension	(89)	Migration and Invasion	(90)
PAK5	Convergence and extension	(91)	Migration	(92)
MARCKS	Convergence and extension	(93)	Migration and Invasion	(94)

704

705 **Table S1.**

706 A list of the fifty genes that play essential role in governing both metastasis and

707 gastrulation progression. The gastrulation defects in Xenopus or zebrafish that are

708 induced by knockdown of each of these genes, were indicated. The molecular

709 mechanism in metastasis that are inhibited by knockdown of each of the same genes,

710 were indicated.

711 **Table S2. A list of the drugs that interfere with epiboly progression in zebrafish**
712

Chemical name	Chemical formula	Effect of 10uM	Effect of 50uM
Acitretin	C21H26O3	Delayed	Delayed
Adrenosterone	C19H24O3	Delayed	Delayed
Albendazole	C12H15N3O2S	Severe delayed	Severe delayed
Alfadolone acetate	C23H34O5	Delayed	Delayed
Alfaxalone	C21H32O3	Delayed	Delayed
Alprostadil	C20H34O5	Delayed	Delayed
Altrenogest	C21H26O2	Slightly delayed	Delayed
Ampiroxicam	C20H21N3O7S	Non effect	Delayed
Anethole-trithione	C10H8OS3	Delayed	Delayed
Antimycin A	C28H40N2O9	Delayed	Delayed
Avobenzone	C20H22O3	Delayed	Delayed
Benzoxiquine	C16H11NO2	Non effect	Delayed
Bosentan	C27H29N5O6S	Delayed	Delayed
Butoconazole nitrate	C19H18Cl3N3O3S	Delayed	Toxic lethal
Camptothecine (S,+)	C20H16N2O4	Severe delayed	Severe delayed
Carbenoxolone disodium salt	C34H48Na2O7	Delayed	Toxic lethal
Carmofur	C11H16FN3O3	Slightly delayed	Delayed
Carprofen	C15H12ClNO2	Severe delayed	Toxic lethal
Cefdinir	C14H13N5O5S2	Delayed	Delayed
Celecoxib	C17H14F3N3O2S	Delayed	Delayed
Chlorambucil	C14H19Cl2NO2	Slightly delayed	Delayed
Chlorhexidine	C22H30Cl2N10	Non effect	Toxic lethal
Ciclopirox ethanolamine	C14H24N2O3	Delayed	Severe delayed
Cinoxacin	C12H10N2O5	Delayed	Severe delayed
Clofibrate	C12H15ClO3	Non effect	Severe delayed
Clopidogrel	C16H16ClNO2S	Non effect	Delayed
Clorgyline hydrochloride	C13H16Cl3NO	Delayed	Delayed
Colchicine	C22H25NO6	Non effect	Delayed
Deptropine citrate	C29H35NO8	Delayed	Delayed
Desipramine hydrochloride	C18H23ClN2	Delayed	Delayed
Diclofenac sodium	C14H10Cl2NNaO2	Delayed	Severe delayed
Dicumarol	C19H12O6	Delayed	Severe delayed
Diethylstilbestrol	C18H20O2	Delayed	Toxic lethal
Dimaprit dihydrochloride	C6H17Cl2N3S	Slightly delayed	Delayed
Disulfiram	C10H20N2S4	Delayed	Delayed
Dopamine hydrochloride	C8H12ClNO2	Delayed	Delayed
Eburnamonine (-)	C19H22N2O	Delayed	Delayed
Ethaverine hydrochloride	C24H30ClNO4	Delayed	Delayed
Ethinylestradiol	C20H24O2	Delayed	Severe delayed
Ethopropazine hydrochloride	C19H25ClN2S	Delayed	Delayed
Ethoxyquin	C14H19NO	Non effect	Delayed
Exemestane	C20H24O2	Slightly delayed	Delayed
Ezetimibe	C24H21F2NO3	Slightly delayed	Delayed
Fenbendazole	C15H13N3O2S	Non effect	Delayed
Fenoprofen calcium salt dihydrate	C30H30CaO8	Slightly delayed	Delayed
Fentiazac	C17H12ClNO2S	Toxic lethal	Toxic lethal
Floxuridine	C9H11FN2O5	Delayed	Toxic lethal
Flunixin meglumine	C21H28F3N3O7	Delayed	Toxic lethal
Flutamide	C11H11F3N2O3	Delayed	Toxic lethal
Fluticasone propionate	C25H31F3O5S	Non effect	Delayed
Furosemide	C12H11ClN2O5S	Delayed	Delayed
Gatifloxacin	C19H22FN3O4	Delayed	Delayed
Gemcitabine	C9H11F2N3O4	Delayed	Delayed
Gemfibrozil	C15H22O3	Delayed	Toxic lethal
Gestrinone	C21H24O2	Delayed	Delayed
Haloprogin	C9H4Cl3IO	Delayed	Toxic lethal
Hexachlorophene	C13H6Cl6O2	Delayed	Severe delayed
Hexestrol	C18H22O2	Slightly delayed	Delayed
Ibudilast	C14H18N2O	Non effect	Delayed
Idazoxan hydrochloride	C11H13ClN2O2	Slightly delayed	Delayed
Idazoxan hydrochloride	C11H13ClN2O2	Non effect	Delayed

Idebenone	C19H30O5	Severe delayed	Toxic lethal
Indomethacin	C19H16ClNO4	Non effect	Delayed
Ipriflavone	C18H16O3	Delayed	Severe delayed
Isotretinoin	C20H28O2	Non effect	Severe delayed
Isradipine	C19H21N3O5	Non effect	Delayed
Lansoprazole	C16H14F3N3O2S	Slightly delayed	Delayed
Latanoprost	C26H40O5	Non effect	Delayed
Leflunomide	C12H9F3N2O2	Delayed	Severe delayed
Letrozole	C17H11N5	Non effect	Delayed
Lithocholic acid	C24H40O3	Non effect	Delayed
Lodoxamide	C11H6ClN3O6	Non effect	Delayed
Lofepramine	C26H27ClN2O	Non effect	Delayed
Loratadine	C22H23ClN2O2	Delayed	Delayed
Loxapine succinate	C22H24ClN3O5	Delayed	Delayed
Mebendazole	C16H13N3O3	Severe delayed	Severe delayed
Mebendazole	C22H26N2O2	Non effect	Delayed
Meloxicam	C14H13N3O4S2	Delayed	Toxic lethal
Methiazole	C12H15N3O2S	Delayed	Delayed
Mevastatin	C23H34O5	Non effect	Delayed
MK 801 hydrogen maleate	C20H19NO4	Slightly delayed	Delayed
Nabumetone	C15H16O2	Non effect	Severe delayed
Naftopidil dihydrochloride	C24H30Cl2N2O3	Slightly delayed	Delayed
Nandrolone	C18H26O2	Delayed	Delayed
Naproxen sodium salt	C14H13NaO3	Delayed	Delayed
Niclosamide	C13H8Cl2N2O4	Delayed	Delayed
Nifekalant	C19H27N5O5	Delayed	Delayed
Niflumic acid	C13H9F3N2O2	Delayed	Delayed
Nimesulide	C13H12N2O5S	Non effect	Delayed
Nisoldipine	C20H24N2O6	Delayed	Toxic lethal
Nitazoxanide	C12H9N3O5S	Severe delayed	Severe delayed
Norethindrone	C20H26O2	Non effect	Delayed
Norgestimate	C23H31NO3	Slightly delayed	Delayed
Oxfendazol	C15H13N3O3S	Slightly delayed	Delayed
Oxibendazol	C12H15N3O3	Severe delayed	Severe delayed
Oxymetholone	C21H32O3	Slightly delayed	Delayed
Parbendazole	C13H17N3O2	Severe delayed	Severe delayed
Parthenolide	C15H20O3	Non effect	Delayed
Penciclovir	C10H15N5O3	Non effect	Delayed
Pentobarbital	C11H18N2O3	Non effect	Delayed
Phenazopyridine hydrochloride	C11H12ClN5	Delayed	Toxic lethal
Phenothiazine	C12H9NS	Non effect	Delayed
Phenoxybenzamine hydrochloride	C18H23Cl2NO	Non effect	Delayed
Pizotifen malate	C23H27NO5S	Delayed	Severe delayed
Pramoxine hydrochloride	C17H28ClNO3	Slightly delayed	Delayed
Prilocaine hydrochloride	C13H21ClN2O	Non effect	Delayed
Primidone	C12H14N2O2	Slightly delayed	Delayed
Racecadotril	C21H23NO4S	Slightly delayed	Delayed
Riluzole hydrochloride	C8H6ClF3N2OS	Non effect	Delayed
Ritonavir	C37H48N6O5S2	Non effect	Severe delayed
S(-)Eticlopride hydrochloride	C17H26Cl2N2O3	Delayed	Delayed
Salmeterol	C25H37NO4	Non effect	Delayed
Streptomycin sulfate	C42H84N14O36S3	Non effect	Delayed
Sulconazole nitrate	C18H16Cl3N3O3S	Delayed	Delayed
Tegafur	C8H9FN2O3	Delayed	Delayed
Telmisartan	C33H30N4O2	Severe delayed	Toxic lethal
Tenatoprazole	C16H18N4O3S	Non effect	Delayed
Terbinafine	C21H25N	Non effect	Delayed
Thimerosal	C9H9HgNaO2S	Non effect	Delayed
Thiorphan	C12H15NO3S	Delayed	Delayed
Tolcapone	C14H11NO5	Severe delayed	Severe delayed
Topotecan	C23H23N3O5	Delayed	Delayed
Tracazolate hydrochloride	C16H25ClN4O2	Severe delayed	Delayed
Tribenoside	C29H34O6	Delayed	Delayed
Triclabendazole	C14H9Cl3N2OS	Delayed	Delayed
Triclosan	C12H7Cl3O2	Delayed	Severe delayed

Trioxsalen	C14H12O3	Delayed	Delayed
Troglitazone	C24H27NO5S	Severe delayed	Toxic lethal
Valproic acid	C8H16O2	Non effect	Delayed
Voriconazole	C16H14F3N5O	Non effect	Delayed
Zardaverine	C12H10F2N2O3	Slightly delayed	Delayed
Zuclopenthixol dihydrochloride	C22H27Cl3N2OS	Delayed	Delayed

713

714 **Table S2. A list of the drugs that interfere with epiboly progression in zebrafish.**

715 Related to Figure 1.

716 A list of positive "hit" drugs that interfered with epiboly progression. Gastrulation

717 defects or status of each of the zebrafish embryos that were treated with either 10μM

718 or 50μM concentrations, are indicated.

719

720

721 **Table S3. Effects of pharmacological inhibition of HTR2C on metastatic**

722 **dissemination of MDA-MB-231 cells in zebrafish xenografted models**

723

		Experiment _#1	Experiment _#2	Experiment _#3	Average of Experiments
Drug: Vehicle Cell: MDA-MB-231	Non-dissemination	0% n1=0/17	0% n2=0/12	6.66% n3=1/15	2.22±3.84%
	Head	58.82% n1=10/17	91.66% n2=11/12	6.66% n3=1/15	72.38±17.15%
	Trunk	52.94% n1=9/17	8.33% n2=1/12	20% n3=2/15	27.09±23.13%
	End-tail	100% n1=17/17	100% n2=12/12	86.66% n3=13/15	95.55±7.69%
Drug: Pizotifen Cell: MDA-MB-231	Non-dissemination	55% n1=11/20	31.57% n2=6/19	45.45 % n3=10/22	44.01±11.77%
	Head	5% n1=1/20	31.57% n2=6/19	18.18% n3=4/22	18.25±13.28%
	Trunk	5% n1=1/20	10.52% n2=2/19	4.45% n3=1/22	6.69±3.32%
	End-tail	45% n1=9/20	57.89% n2=11/19	50% n3=11/22	50.96±6.50%

724

725 Related to Figure 2D.

726 The numbers and frequencies of the fish showing the dissemination patterns in vehicle

727 or Pizotifen-treated group, were indicated. The fish showed both patterns of

728 dissemination were redundantly counted in this analysis.

729

730 **Table S4. Effects of pharmacological inhibition of HTR2C on metastatic**

731 **dissemination of Mia-PaCa2 cells in zebrafish xenografted models**

732

		Experiment _#1	Experiment _#2	Average of Experiments
Drug: Vehicle Cell: MIA-PaCa2	Non-dissemination	17.64% n1=3/17	16.66% n2=2/12	17.15+0.69%
	Head	82.35% n1=14/17	66.66% n2=8/12	74.50+11.09%
	Trunk	29.41% n1=5/17	8.33% n2=1/12	18.87+14.90%
	End-tail	70.58% n1=12/17	83.33% n2=10/17	76.96%+9.01
Drug: Pizotifen Cell: MIA-PaCa2	Non-dissemination	40% n1=4/10	52.63% n2=10/19	46.31+8.93%
	Head	20% n1=2/10	10.52% n2=2/19	15.26+6.69%
	Trunk	10% n1=1/10	5.26% n2=1/19	7.63+3.34%
	End-tail	40% n1=4/10	42.05% n2=8/19	41.4+1.48%

733

734 Related to Figure S3.

735 The numbers and frequencies of the fish showing the dissemination patterns in vehicle

736 or Pizotifen-treated group, were indicated. The fish showed both patterns of

737 dissemination were redundantly counted in this analysis.

738 **Table S5. Effects of genetic inhibition of HTR2C on metastatic dissemination of**

739 **MDA-MB-231 cells in zebrafish xenografted models**

740

		Experiment _#1	Experiment _#2	Average of Experiments
shLacZ	Non-dissemination	0% n1=0/10	0% n2=0/10	0%
	Head	60% n1=6/10	100% n2=10/10	80 ±28.28%
	Trunk	30% n1=3/10	10% n2=1/10	20±14.14%
	End-tail	80% n1=8/10	100% n2=10/10	90%±14.14
shHTR2C	Non-dissemination	80% n1=12/15	76.84% n2=14/19	76.84±4.46 %
	Head	6.66% n1=1/15	15.78% n2=3/19	11.22±6.45%
	Trunk	6.66% n1=1/15	5.26% n2=1/19	5.96±0.99%
	End-tail	20% n1=3/15	26.31% n2=5/19	23.15±4.46%

741

742 Related to Figure 2E.

743 The numbers and frequencies of the fish showing the dissemination patterns in the

744 zebrafish that were inoculated with either shLacZ or shHTR2C MDA-MB-231 cells,

745 were indicated. The fish showed both patterns of dissemination were redundantly

746 counted in this analysis.

747 **Table S6. Effects of HTR2C overexpression on metastatic dissemination of**

748 **MCF7 cells in zebrafish xenografted models**

749

		Experiment _#1	Experiment _#2	Average of Experiments
VC	Non-dissemination	46.15% n1=6/13	40% n2=4/10	43.07±4.35%
	Head	46.15% n1=6/13	20% n2=2/10	33.07±18.49%
	Trunk	0% n1=0/13	0% n2=0/10	0%
	End-tail	53.84% n1=7/13	60% n2=6/10	56.92±4.35
HTR2C	Non-dissemination	0% n1=0/14	0% n2=0/15	0%
	Head	100% n1=14/14	93.33% n2=14/15	96.66±4.71%
	Trunk	64.28% n1=9/14	73.33% n2=11/15	68.80±6.39%
	End-tail	85.71% n1=12/14	93.33% n2=14/15	89.52±5.38%

750

751 Related to Figure 4E.

752 The numbers and frequencies of the fish showing the dissemination patterns in the

753 zebrafish that were inoculated with MCF7 cells expressing either VC or HTR2C, were

754 indicated. The fish showed both patterns of dissemination were redundantly counted

755 in this analysis.

756

757 **References for Table S1.**

758 1. Kondo M (2007) Bone morphogenetic proteins in the early development of
759 zebrafish. *FEBS J* 274(12):2960-2967.
760 2. Katsuno Y, *et al.* (2008) Bone morphogenetic protein signaling enhances
761 invasion and bone metastasis of breast cancer cells through Smad pathway.
762 *Oncogene* 27(49):6322-6333.
763 3. Tada M & Smith JC (2000) Xwnt11 is a target of Xenopus Brachyury:
764 regulation of gastrulation movements via Dishevelled, but not through the
765 canonical Wnt pathway. *Development* 127:2227-2238.
766 4. Vincan E & Barker N (2008) The upstream components of the Wnt signalling
767 pathway in the dynamic EMT and MET associated with colorectal cancer
768 progression. *Clin Exp Metastasis* 25(6):657-663.
769 5. Yang X, Dormann D, Munsterberg AE, & Weijer CJ (2002) Cell movement
770 patterns during gastrulation in the chick are controlled by positive and
771 negative chemotaxis mediated by FGF4 and FGF8. *Dev Cell* 3(3):425-437.
772 6. Nomura S, *et al.* (2008) FGF10/FGFR2 signal induces cell migration and
773 invasion in pancreatic cancer. *Br J Cancer* 99(2):305-313.

774 7. Song S, *et al.* (2013) Pou5f1-dependent EGF expression controls E-cadherin
775 endocytosis, cell adhesion, and zebrafish epiboly movements. *Dev Cell*
776 24(5):486-501.
777 8. Lu Z, Jiang G, Blume-Jensen P, & Hunter T (2001) Epidermal growth factor-
778 induced tumor cell invasion and metastasis initiated by dephosphorylation
779 and downregulation of focal adhesion kinase. *Mol Cell Biol* 21(12):4016-4031.
780 9. Damm EW & Winklbauer R (2011) PDGF-A controls mesoderm cell
781 orientation and radial intercalation during Xenopus gastrulation.
782 *Development* 138(3):565-575.
783 10. Jechlinger M, *et al.* (2006) Autocrine PDGFR signaling promotes mammary
784 cancer metastasis. *J Clin Invest* 116(6):1561-1570.
785 11. Mizoguchi T, Verkade H, Heath JK, Kuroiwa A, & Kikuchi Y (2008) Sdf1/Cxcr4
786 signaling controls the dorsal migration of endodermal cells during zebrafish
787 gastrulation. *Development* 135(15):2521-2529.
788 12. Shen HB, Gu ZQ, Jian K, & Qi J (2013) CXCR4-mediated Stat3 activation is
789 essential for CXCL12-induced cell invasion in bladder cancer. *Tumour Biol*
790 34(3):1839-1845.
791 13. Montero J-A, Kilian B, Chan J, Bayliss PE, & Heisenberg C-P (2003)
792 Phosphoinositide 3-Kinase Is Required for Process Outgrowth and Cell
793 Polarization of Gastrulating Mesendodermal Cells. *Current Biology*
794 13(15):1279-1289.
795 14. Wander SA, *et al.* (2013) PI3K/mTOR inhibition can impair tumor invasion
796 and metastasis in vivo despite a lack of antiproliferative action in vitro:
797 implications for targeted therapy. *Breast Cancer Res Treat* 138(2):369-381.
798 15. Tsai WB, Zhang X, Sharma D, Wu W, & Kinsey WH (2005) Role of Yes kinase
799 during early zebrafish development. *Dev Biol* 277(1):129-141.
800 16. Barraclough J, Hodgkinson C, Hogg A, Dive C, & Welman A (2007) Increases in
801 c-Yes Expression Level and Activity Promote Motility But Not Proliferation of
802 Human Colorectal Carcinoma Cells. *Neoplasia* 9(9):745-IN732.
803 17. Sharma D, Holets L, Zhang X, & Kinsey WH (2005) Role of Fyn kinase in
804 signaling associated with epiboly during zebrafish development. *Dev Biol*
805 285(2):462-476.
806 18. Yadav V & Denning MF (2011) Fyn is induced by Ras/PI3K/Akt signaling and
807 is required for enhanced invasion/migration. *Mol Carcinog* 50(5):346-352.
808 19. Krens SF, *et al.* (2008) Distinct functions for ERK1 and ERK2 in cell migration
809 processes during zebrafish gastrulation. *Dev Biol* 319(2):370-383.
810 20. Radtke S, Milanovic M, & Rossé C (2013) ERK2 but not ERK1 mediates HGF-
811 induced motility in non-small cell lung carcinoma cell lines. *J Cell Sci.*
812 126(Pt11):2381-2391.
813 21. Jopling C, van Geemen D, & den Hertog J (2007) Shp2 knockdown and
814 Noonan/LEOPARD mutant Shp2-induced gastrulation defects. *PLoS Genet*
815 3(12):e225.
816 22. Wang FM, *et al.* (2005) SHP-2 promoting migration and metastasis of MCF-7
817 with loss of E-cadherin, dephosphorylation of FAK and secretion of MMP-9
818 induced by IL-1beta in vivo and in vitro. *Breast Cancer Res Treat* 89(1):5-14.
819 23. Ip YT & Gridley T (2002) Cell movements during gastrulation: snail
820 dependent and independent pathways. *Curr Opin Genet Dev* 12(4):423-429.
821 24. Batlle E, Sancho E, Francí C, Domínguez D, & Monfar M (2000) The
822 transcription factor snail is a repressor of E-cadherin gene expression in
823 epithelial tumour cells. *Nat Cell Biol* 2(2):84-89.
824 25. Shi J, Severson C, Yang J, Wedlich D, & Klymkowsky MW (2011) Snail2
825 controls mesodermal BMP/Wnt induction of neural crest. *Development*
826 138(15):3135-3145.

827 26. Castanon I & Baylies MK (2002) A Twist in fate: evolutionary comparison of
828 Twist structure and function. *Gene* 287(1-2):11-22.
829 27. Yang J, *et al.* (2004) Twist, a master regulator of morphogenesis, plays an
830 essential role in tumor metastasis. *Cell* 117(7):927-939.
831 28. Fernando RI, *et al.* (2010) The T-box transcription factor Brachyury
832 promotes epithelial-mesenchymal transition in human tumor cells. *J Clin*
833 *Invest* 120(2):533-544.
834 29. Vannier C, Mock K, Brabletz T, & Driever W (2013) Zeb1 regulates E-cadherin
835 and Epcam (epithelial cell adhesion molecule) expression to control cell
836 behavior in early zebrafish development. *J Biol Chem* 288(26):18643-18659.
837 30. Spaderna S, *et al.* (2008) The transcriptional repressor ZEB1 promotes
838 metastasis and loss of cell polarity in cancer. *Cancer Res* 68(2):537-544.
839 31. Sander V, Reversade B, & De Robertis EM (2007) The opposing homeobox
840 genes Goosecoid and Vent1/2 self-regulate Xenopus patterning. *EMBO J*
841 26(12):2955-2965.
842 32. Hartwell KA, *et al.* (2006) The Spemann organizer gene, Goosecoid, promotes
843 tumor metastasis. *Proc Natl Acad Sci U S A* 103(50):18969-18974.
844 33. Wilm B, James RG, Schultheiss TM, & Hogan BL (2004) The forkhead genes,
845 Foxc1 and Foxc2, regulate paraxial versus intermediate mesoderm cell fate.
846 *Dev Biol* 271(1):176-189.
847 34. Mani SA, *et al.* (2007) Mesenchyme Forkhead 1 (FOXC2) plays a key role in
848 metastasis and is associated with aggressive basal-like breast cancers. *Proc*
849 *Natl Acad Sci U S A* 104(24):10069-10074.
850 35. Miyagi C, *et al.* (2004) STAT3 noncell-autonomously controls planar cell
851 polarity during zebrafish convergence and extension. *J Cell Biol* 166(7):975-
852 981.
853 36. Abdulghani J, *et al.* (2008) Stat3 promotes metastatic progression of prostate
854 cancer. *Am J Pathol* 172(6):1717-1728.
855 37. Lachnit M, Kur E, & Driever W (2008) Alterations of the cytoskeleton in all
856 three embryonic lineages contribute to the epiboly defect of Pou5f1/Oct4
857 deficient MZspg zebrafish embryos. *Dev Biol* 315(1):1-17.
858 38. Dai X, *et al.* (2013) OCT4 regulates epithelial-mesenchymal transition and its
859 knockdown inhibits colorectal cancer cell migration and invasion. *Oncol Rep*
860 29(1):155-160.
861 39. O'Carroll D, *et al.* (2001) The polycomb-group gene Ezh2 is required for early
862 mouse development. *Mol Cell Biol* 21(13):4330-4336.
863 40. Ren G, *et al.* (2012) Polycomb protein EZH2 regulates tumor invasion via the
864 transcriptional repression of the metastasis suppressor RKIP in breast and
865 prostate cancer. *Cancer Res* 72(12):3091-3104.
866 41. Lin F, *et al.* (2005) Essential roles of G{alpha}12/13 signaling in distinct cell
867 behaviors driving zebrafish convergence and extension gastrulation
868 movements. *J Cell Biol* 169(5):777-787.
869 42. Chen MW, *et al.* (2010) H3K9 histone methyltransferase G9a promotes lung
870 cancer invasion and metastasis by silencing the cell adhesion molecule Ep-
871 CAM. *Cancer Res* 70(20):7830-7840.
872 43. van der Lugt NM, *et al.* (1994) Posterior transformation, neurological
873 abnormalities, and severe hematopoietic defects in mice with a targeted
874 deletion of the bmi-1 proto-oncogene. *Genes Dev* 8(7):757-769.
875 44. Guo BH, *et al.* (2011) Bmi-1 promotes invasion and metastasis, and its
876 elevated expression is correlated with an advanced stage of breast cancer.
877 *Mol Cancer* 10(1):10.
878 45. Zhu S, Liu L, Korzh V, Gong Z, & Low BC (2006) RhoA acts downstream of
879 Wnt5 and Wnt11 to regulate convergence and extension movements by

880 involving effectors Rho kinase and Diaphanous: use of zebrafish as an in vivo
881 model for GTPase signaling. *Cell Signal* 18(3):359-372.
882 46. Yoshioka K, Nakamori S, & Itoh K (1999) Overexpression of small GTP-
883 binding protein RhoA promotes invasion of tumor cells. *Cancer Res*
884 59(8):2004-2010.
885 47. Choi SC & Han JK (2002) Xenopus Cdc42 regulates convergent extension
886 movements during gastrulation through Wnt/Ca2+ signaling pathway. *Dev*
887 *Biol* 244(2):342-357.
888 48. Reymond N, *et al.* (2012) Cdc42 promotes transendothelial migration of
889 cancer cells through beta1 integrin. *J Cell Biol* 199(4):653-668.
890 49. Habas R, Dawid IB, & He X (2003) Coactivation of Rac and Rho by
891 Wnt/Frizzled signaling is required for vertebrate gastrulation. . *Genes Dev*
892 17(2):295-309.
893 50. Vega FM & Ridley AJ (2008) Rho GTPases in cancer cell biology. *FEBS Lett*
894 582(14):2093-2101.
895 51. Marlow F, Topczewski J, Sepich D, & Solnica-Krezel L (2002) Zebrafish Rho
896 kinase 2 acts downstream of Wnt11 to mediate cell polarity and effective
897 convergence and extension movements. *Curr Biol* 12(11):876-884.
898 52. Itoh K, *et al.* (1999) An essential part for Rho-associated kinase in the
899 transcellular invasion of tumor cells. *Nat Med* 5(2):221-225.
900 53. Kusakabe M & Nishida E (2004) The polarity-inducing kinase Par-1 controls
901 Xenopus gastrulation in cooperation with 14-3-3 and aPKC. *EMBO J*
902 23(21):4190-4201.
903 54. Shi X, Gangadharan B, Brass LF, Ruf W, & Mueller BM (2004) Protease-
904 activated receptors (PAR1 and PAR2) contribute to tumor cell motility and
905 metastasis. *Mol Cancer Res* 2(7):395-402.
906 55. Gunaratne A, Thai BL, & Di Guglielmo GM (2013) Atypical protein kinase C
907 phosphorylates Par6 and facilitates transforming growth factor beta-induced
908 epithelial-to-mesenchymal transition. *Mol Cell Biol* 33(5):874-886.
909 56. Seifert K, Ibrahim H, Stodtmeister T, Winklbauer R, & Niessen CM (2009) An
910 adhesion-independent, aPKC-dependent function for cadherins in
911 morphogenetic movements. *J Cell Sci* 122(Pt 14):2514-2523.
912 57. Yamazaki K, *et al.* (2009) Adenylate cyclase-associated protein 1
913 overexpressed in pancreatic cancers is involved in cancer cell motility. *Lab*
914 *Invest* 89(4):425-432.
915 58. Link V, *et al.* (2006) Identification of regulators of germ layer morphogenesis
916 using proteomics in zebrafish. *J Cell Sci* 119(Pt 10):2073-2083.
917 59. Khanna C, *et al.* (2004) The membrane-cytoskeleton linker ezrin is necessary
918 for osteosarcoma metastasis. *Nat Med* 10(2):182-186.
919 60. Slanchev K, *et al.* (2009) The epithelial cell adhesion molecule EpCAM is
920 required for epithelial morphogenesis and integrity during zebrafish epiboly
921 and skin development. *PLoS Genet* 5(7):e1000563.
922 61. Ni J, *et al.* (2012) Role of the EpCAM (CD326) in prostate cancer metastasis
923 and progression. *Cancer Metastasis Rev* 31(3-4):779-791.
924 62. Skalski M, Alfandari D, & Darribere T (1998) A key function for alphav
925 containing integrins in mesodermal cell migration during Pleurodeles waltl
926 gastrulation. *Dev Biol* 195(2):158-173.
927 63. Felding-Habermann B (2003) Integrin adhesion receptors in tumor
928 metastasis. *Clin Exp Metastasis* 20(3):203-213.
929 64. Marsden M & DeSimone DW (2003) Integrin-ECM Interactions Regulate
930 Cadherin-Dependent Cell Adhesion and Are Required for Convergent
931 Extension in Xenopus. *Current Biology* 13(14):1182-1191.

932 65. Malik G, *et al.* (2010) Plasma fibronectin promotes lung metastasis by
933 contributions to fibrin clots and tumor cell invasion. *Cancer Res* 70(11):4327-
934 4334.
935 66. Bakkers J, *et al.* (2004) Has2 is required upstream of Rac1 to govern dorsal
936 migration of lateral cells during zebrafish gastrulation. *Development*
937 131(3):525-537.
938 67. Kim HR, *et al.* (2004) Hyaluronan facilitates invasion of colon carcinoma cells
939 in vitro via interaction with CD44. *Cancer Res* 64(13):4569-4576.
940 68. Coyle RC, Latimer A, & Jessen JR (2008) Membrane-type 1 matrix
941 metalloproteinase regulates cell migration during zebrafish gastrulation:
942 evidence for an interaction with non-canonical Wnt signaling. *Exp Cell Res*
943 314(10):2150-2162.
944 69. Perentes JY, *et al.* (2011) Cancer cell-associated MT1-MMP promotes blood
945 vessel invasion and distant metastasis in triple-negative mammary tumors.
946 *Cancer Res* 71(13):4527-4538.
947 70. Cha YI, *et al.* (2006) Cyclooxygenase-1-derived PGE2 promotes cell motility
948 via the G-protein-coupled EP4 receptor during vertebrate gastrulation. *Genes*
949 *Dev* 20(1):77-86.
950 71. Kundu N & Fulton AM (2002) Selective cyclooxygenase (COX)-1 or COX-2
951 inhibitors control metastatic disease in a murine model of breast cancer.
952 *Cancer Res* 62(8):2343-2346.
953 72. Speirs CK, *et al.* (2010) Prostaglandin Gbetagamma signaling stimulates
954 gastrulation movements by limiting cell adhesion through Snai1a
955 stabilization. *Development* 137(8):1327-1337.
956 73. Wang D & Dubois RN (2006) Prostaglandins and cancer. *Gut* 55(1):115-122.
957 74. Yamashita S, *et al.* (2004) Zinc transporter LIVI controls epithelial-
958 mesenchymal transition in zebrafish gastrula organizer. *Nature*
959 429(6989):298-302.
960 75. Lue HW, *et al.* (2011) LIV-1 promotes prostate cancer epithelial-to-
961 mesenchymal transition and metastasis through HB-EGF shedding and EGFR-
962 mediated ERK signaling. *PLoS One* 6(11):e27720.
963 76. Yagi H, *et al.* (2011) A synthetic biology approach reveals a CXCR4-G13-Rho
964 signaling axis driving transendothelial migration of metastatic breast cancer
965 cells. *Sci Signal* 4(191):ra60.
966 77. Webster DM, *et al.* (2009) O-GlcNAc modifications regulate cell survival and
967 epiboly during zebrafish development. *BMC Dev Biol* 9:28.
968 78. Lynch TP, *et al.* (2012) Critical role of O-Linked beta-N-acetylglucosamine
969 transferase in prostate cancer invasion, angiogenesis, and metastasis. *J Biol*
970 *Chem* 287(14):11070-11081.
971 79. Latinkic BV (2003) Xenopus Cyr61 regulates gastrulation movements and
972 modulates Wnt signalling. *Development* 130(11):2429-2441.
973 80. Lin J, *et al.* (2012) A novel anti-Cyr61 antibody inhibits breast cancer growth
974 and metastasis in vivo. *Cancer Immunol Immunother* 61(5):677-687.
975 81. Liu W, *et al.* (2011) TRPM7 regulates gastrulation during vertebrate
976 embryogenesis. *Dev Biol* 350(2):348-357.
977 82. Middelbeek J, *et al.* (2012) TRPM7 is required for breast tumor cell
978 metastasis. *Cancer Res* 72(16):4250-4261.
979 83. Holloway BA, *et al.* (2009) A novel role for MAPKAPK2 in morphogenesis
980 during zebrafish development. *PLoS Genet* 5(3):e1000413.
981 84. Kumar B, *et al.* (2010) p38 mitogen-activated protein kinase-driven
982 MAPKAPK2 regulates invasion of bladder cancer by modulation of MMP-2
983 and MMP-9 activity. *Cancer Res* 70(2):832-841.

984 85. Machingo QJ, Fritz A, & Shur BD (2006) A beta1,4-galactosyltransferase is
985 required for convergent extension movements in zebrafish. *Dev Biol*
986 297(2):471-482.
987 86. Zhu X*, et al.* (2005) Elevated beta1,4-galactosyltransferase I in highly
988 metastatic human lung cancer cells. Identification of E1AF as important
989 transcription activator. *J Biol Chem* 280(13):12503-12516.
990 87. Hong SK, Tanegashima K, & Dawid IB (2011) XIer2 is required for convergent
991 extension movements during Xenopus development. *Int J Dev Biol* 55(10-
992 12):917-921.
993 88. Neeb A*, et al.* (2012) The immediate early gene Ier2 promotes tumor cell
994 motility and metastasis, and predicts poor survival of colorectal cancer
995 patients. *Oncogene* 31(33):3796-3806.
996 89. Besser J, Leito JT, van der Meer DL, & Bagowski CP (2007) Tip-1 induces
997 filopodia growth and is important for gastrulation movements during
998 zebrafish development. *Dev Growth Differ* 49(3):205-214.
999 90. Han M, Wang H, Zhang HT, & Han Z (2012) The PDZ protein TIP-1 facilitates
1000 cell migration and pulmonary metastasis of human invasive breast cancer
1001 cells in athymic mice. *Biochem Biophys Res Commun* 422(1):139-145.
1002 91. Faure S*, et al.* (2005) Xenopus p21-activated kinase 5 regulates blastomeres'
1003 adhesive properties during convergent extension movements. *Dev Biol*
1004 277(2):472-492.
1005 92. Gong W*, et al.* (2009) P21-activated kinase 5 is overexpressed during
1006 colorectal cancer progression and regulates colorectal carcinoma cell
1007 adhesion and migration. *Int J Cancer* 125(3):548-555.
1008 93. Iioka H, Ueno N, & Kinoshita N (2004) Essential role of MARCKS in cortical
1009 actin dynamics during gastrulation movements. *J Cell Biol* 164(2):169-174.
1010 94. Rombouts K*, et al.* (2013) Myristoylated Alanine-Rich protein Kinase C
1011 Substrate (MARCKS) expression modulates the metastatic phenotype in
1012 human and murine colon carcinoma in vitro and in vivo. *Cancer Lett*
1013 333(2):244-252.
1014 95. Medici D, Hay ED, & B.R. O (2008) Snail and Slug Promote Epithelial-
1015 Mesenchymal Transition through -Catenin–T-Cell Factor-4-dependent Expression
1016 of Transforming Growth Factor-3. Molecular Biology of the Cell 19(11):4875–
1017 4887.

1018 **Source data and legend for source data**

1019

1020

1021 **Figure 2a_HRT2C_source data**

1022

1023

1024 Western blot analysis of HRT2C protein levels in non-metastatic human cancer cell

1025 line, MCF7 (breast) and highly metastatic human cancer cell lines, MDA-MB-231

1026 (breast), MDA-MB-435 (melanoma), MIA-PaCa2 (pancreas), SW620 (colon) and

1027 PC3 (prostate).

1028

1029 **Figure 2a_GAPDH_source data**

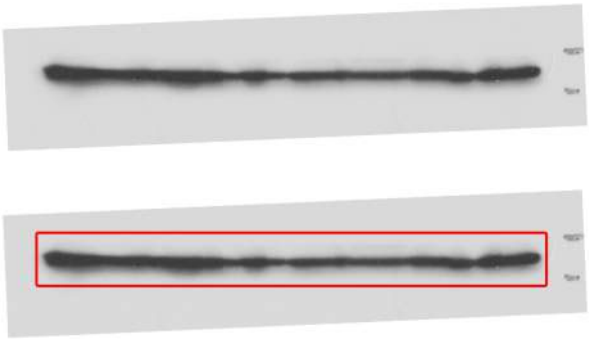

1030

1031

1032 Western blot analysis of GAPDH protein levels in non-metastatic human cancer cell

1033 line, MCF7 (breast) and highly metastatic human cancer cell lines, MDA-MB-231

1034 (breast), MDA-MB-435 (melanoma), MIA-PaCa2 (pancreas), SW620 (colon) and

1035 PC3 (prostate).

1036

1037 **Figure 4C_E-cadherin in MCF7_ source data**

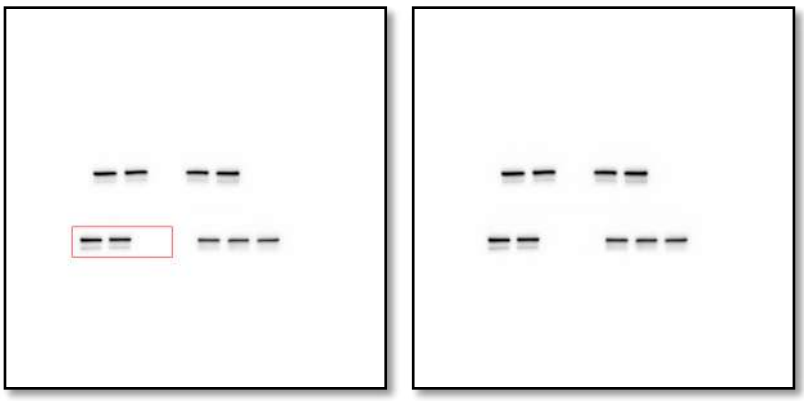

Western blot analysis of E-cadherin protein levels in MCF7 cells expressing either the control vector or HTR2C.

Figure 4C_EpCAM in MCF7_ source data

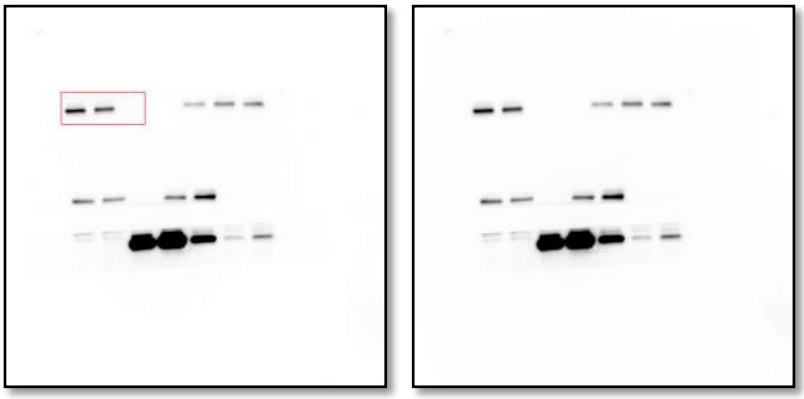

Western blot analysis of EpCAM protein levels in MCF7 cells expressing either the control vector or HTR2C.

Figure 4C_Vimentin in MCF7_ source data

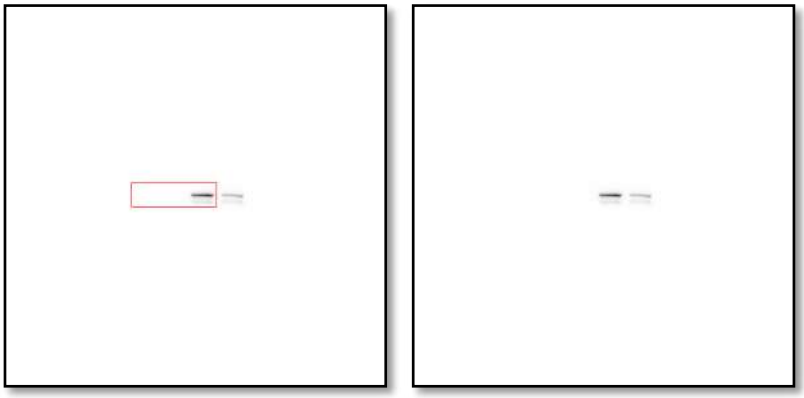

1049 Western blot analysis of Vimentin protein levels in MCF7 cells expressing either the

1050 control vector or HTR2C.

1051

1052 **Figure 4C_N-cadherin in MCF7_ source data**

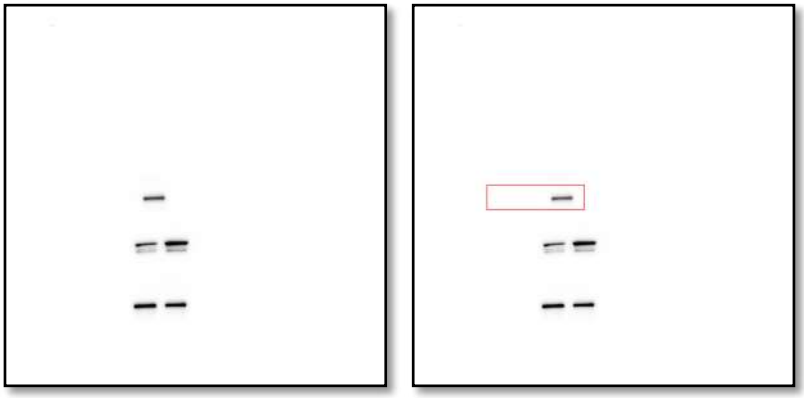

1053

1054 Western blot analysis of N-cadherin protein levels in MCF7 cells expressing either the

1055 control vector or HTR2C.

1056

1057 **Figure 4C_Zeb1 in MCF7_ source data**

1058

1059 Western blot analysis of Zeb1 protein levels in MCF7 cells expressing either the

1060 control vector or HTR2C.

1061

1062 **Figure 4C_HRT2C in MCF7_ source data**

Western blot analysis of HRT2C protein levels in MCF7 cells expressing either the control vector or HTR2C.

Figure 4C_GAPDH in MCF7_source data

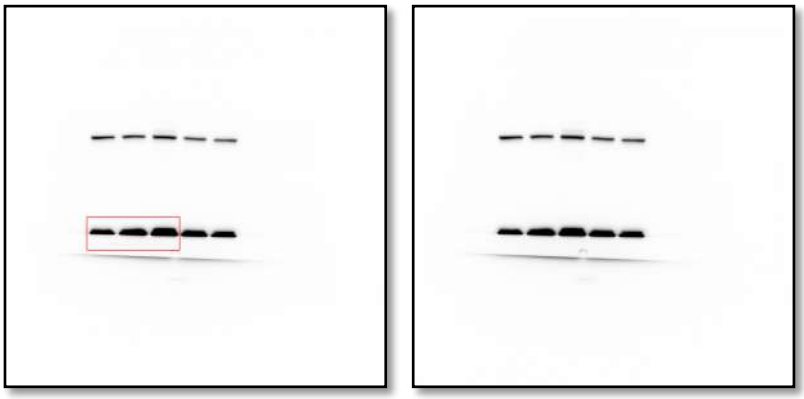

Western blot analysis of GAPDH protein levels in MCF7 cells expressing either the control vector or HTR2C.

Figure 4C_E-cadherin in HaCaT_source data

1074 Western blot analysis of E-cadherin protein levels in HaCaT cells expressing either

1075 the control vector or HTR2C.

1076

1077 **Figure 4C_EpCAM in HaCaT_source data**

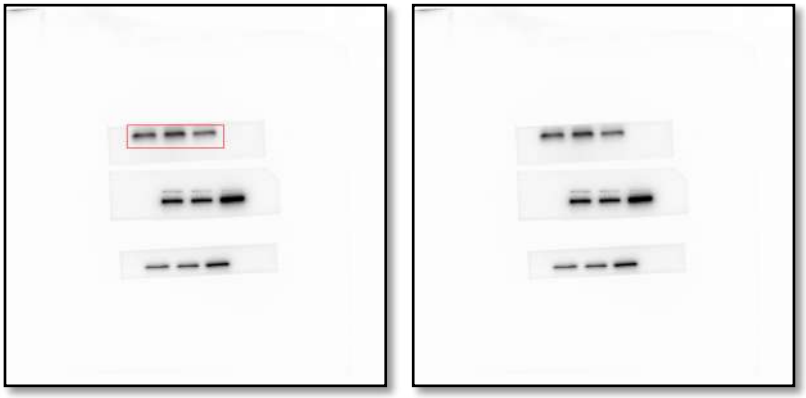

1078

1079 Western blot analysis of EpCAM protein levels in HaCaT cells expressing either the

1080 control vector or HTR2C.

1081

1082 **Figure 4C_Vimentin in HaCaT_source data**

1083

1084 Western blot analysis of Vimentin protein levels in HaCaT cells expressing either the

1085 control vector or HTR2C.

1086

1087 **Figure 4C_N-cadherin in HaCaT_source data**

Western blot analysis of N-cadherin protein levels in HaCaT cells expressing either the control vector or HTR2C.

Figure 4C_Zeb1 in HaCaT source data

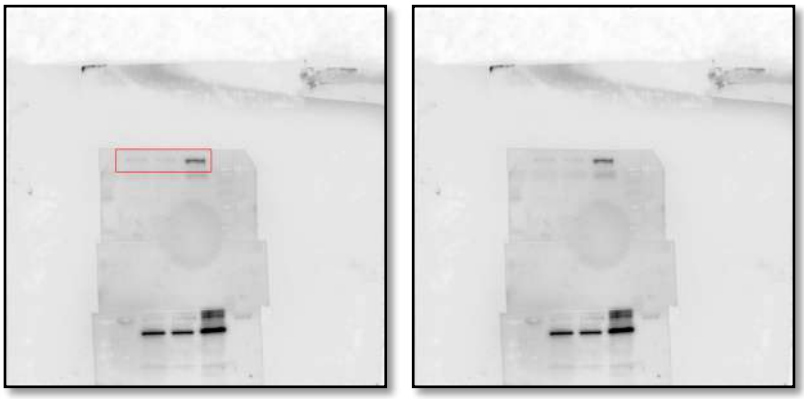

Western blot analysis of zeb1 protein levels in HaCaT cells expressing either the control vector or HTR2C.

Figure 4C_HRT2C in HaCaT_source data

1099 Western blot analysis of HRT2C protein levels in HaCaT cells expressing either the

1100 control vector or HTR2C.

1101

1102 **Figure 4C_GAPDH in HaCaT_source data**

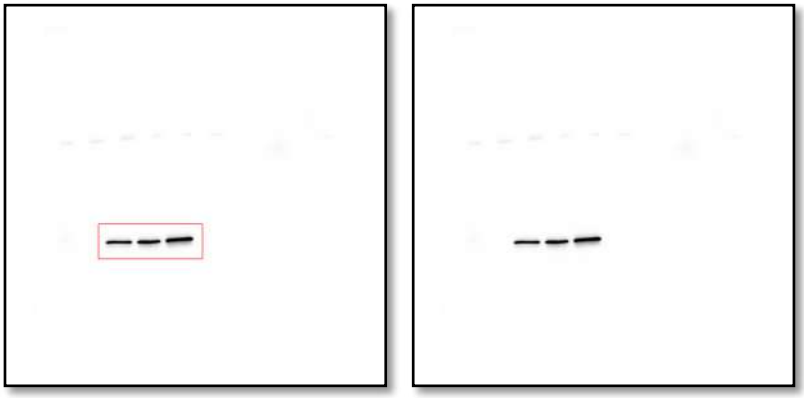

1103

1104 Western blot analysis of GAPDH protein levels in HaCaT cells expressing either the

1105 control vector or HTR2C.

1106

1107 **Figure 5C_E-cadherin_source data**

1108

1109 Western blot analysis of E-cadherin protein levels in whole cell lysate of 4T1 primary

1110 tumors from either vehicle or Pizotifen-treated mice.

1111

1112 **Figure 5C_Zeb1 _source data**

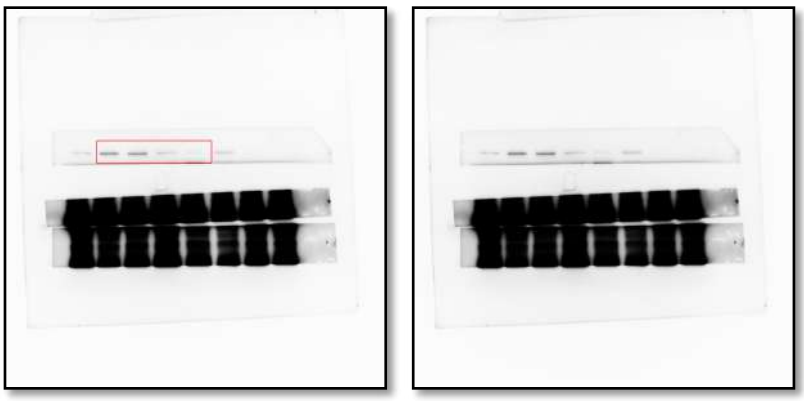

Western blot analysis of Zeb1 protein levels in whole cell lysate of 4T1 primary tumors from either vehicle or Pizotifen-treated mice.

Figure 5C_ Phosphorylation of serine-9 in GSK3β_source data

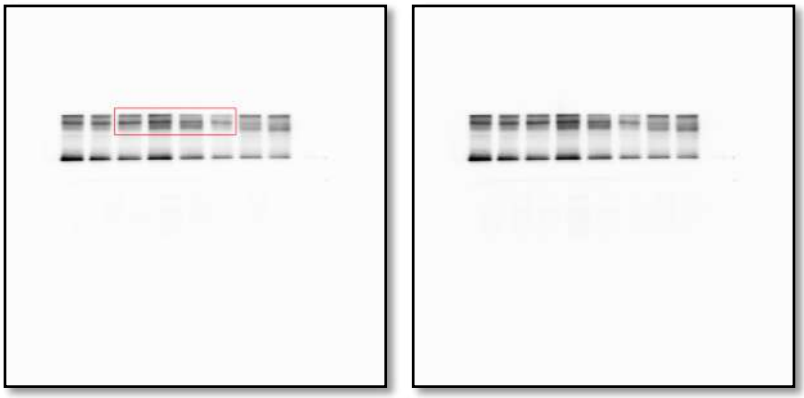

Western blot analysis of the protein levels of phosphorylation of serine-9 in GSK3β in whole cell lysate of 4T1 primary tumors from either vehicle or Pizotifen-treated mice.

Figure 5C_ GSK3β_source data

1124 Western blot analysis of GSK3β protein levels in whole cell lysate of 4T1 primary

1125 tumors from either vehicle or Pizotifen-treated mice.

1126

1127 **Figure 5C_Luciferase_source data**

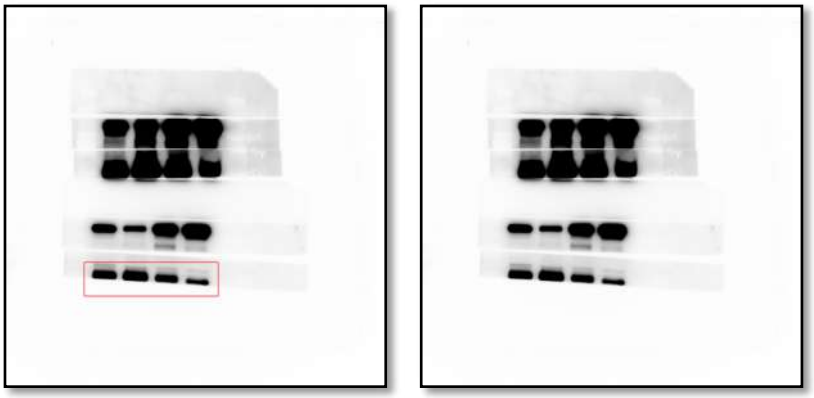

1128

1129 Western blot analysis of Luciferase protein levels in whole cell lysate of 4T1 primary

1130 tumors from either vehicle or Pizotifen-treated mice.

1131

1132 **Figure 5C_β-catenin in the nucleus_source data**

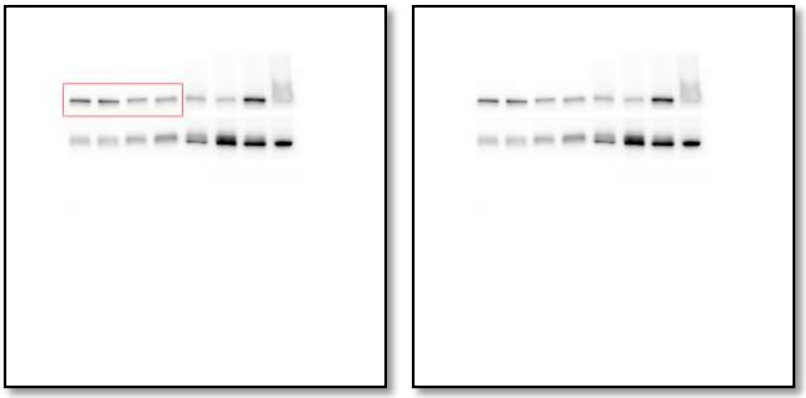

1133

1134 Western blot analysis of β-catenin protein levels in the nucleus of 4T1 primary tumors

1135 from either vehicle or Pizotifen-treated mice.

1136

1137 **Figure 5C_Histone H3 in the nucleus_source data**

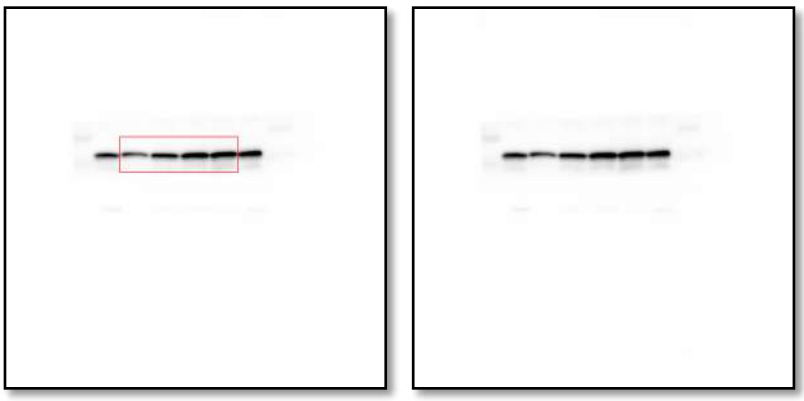

Western blot analysis of Histone H3 protein levels in the nucleus of 4T1 primary tumors from either vehicle or Pizotifen-treated mice.

Figure 5C_β-catenin in the cytoplasm_source data

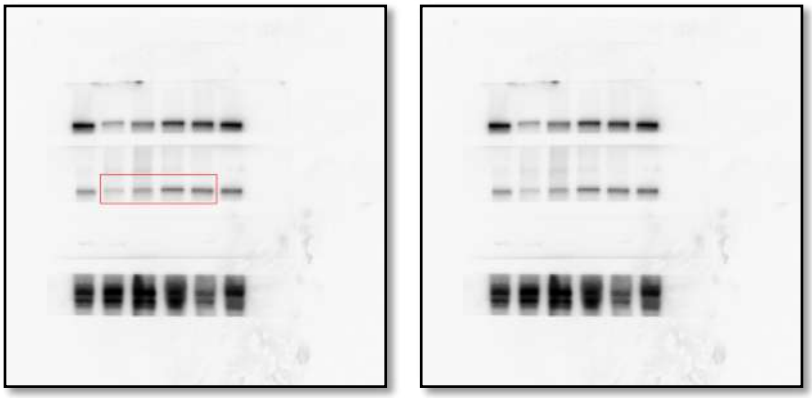

Western blot analysis of β-catenin protein levels in the cytoplasm of 4T1 primary tumors from either vehicle or Pizotifen-treated mice.

Figure 5C_β-tubulin in the cytoplasm_source data

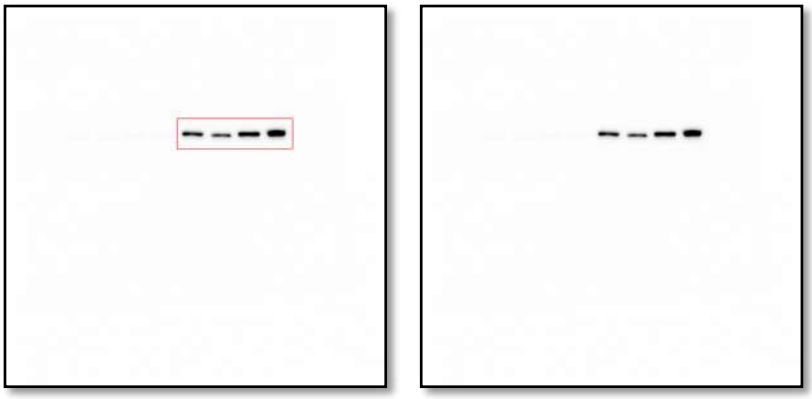

1149 Western blot analysis of β-tubulin protein levels in the cytoplasm of 4T1 primary

1150 tumors from either vehicle or Pizotifen-treated mice.

1151

1152 **Figure 5D_E-cadherin_source data**

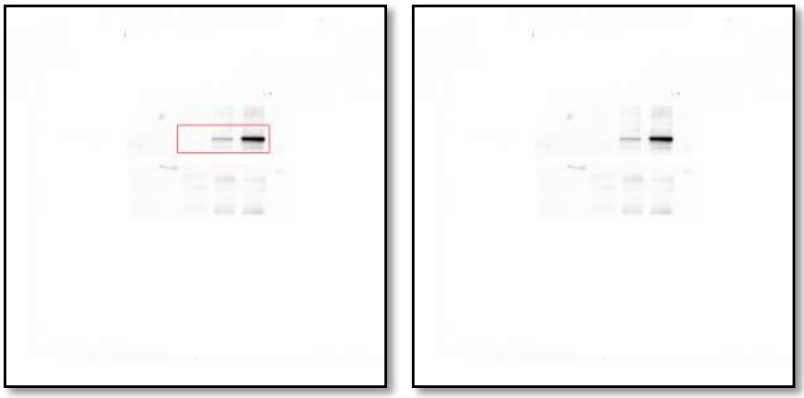

1153

1154 Western blot analysis of E-cadherin protein levels in either vehicle or Pizotifen-treated

1155 MDA-MB-231 cells or E-cadherin positive cells in Pizotifen-treated MDA-MB-231

1156 cells.

1157

1158 **Figure 5D_EpCAM_source data**

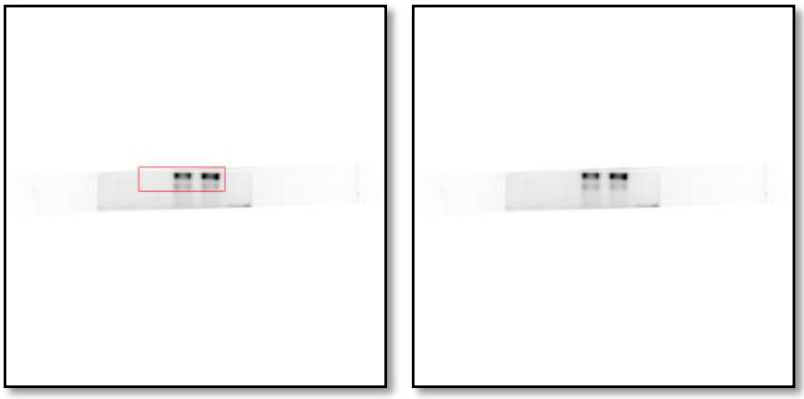

1159

1160 Western blot analysis of EpCAM protein levels in either vehicle or Pizotifen-treated

1161 MDA-MB-231 cells or E-cadherin positive cells in Pizotifen-treated MDA-MB-231

1162 cells.

1163

1164 **Figure 5D_Keratin18 (KRT18)_source data**

Western blot analysis of KRT18 protein levels in either vehicle or Pizotifen-treated MDA-MB-231 cells or E-cadherin positive cells in Pizotifen-treated MDA-MB-231 cells.

Figure 5D_Keratin19 (KRT19)_source data

Western blot analysis of KRT19 protein levels in either vehicle or Pizotifen-treated MDA-MB-231 cells or E-cadherin positive cells in Pizotifen-treated MDA-MB-231 cells.

Figure 5D_Vimentin_source data

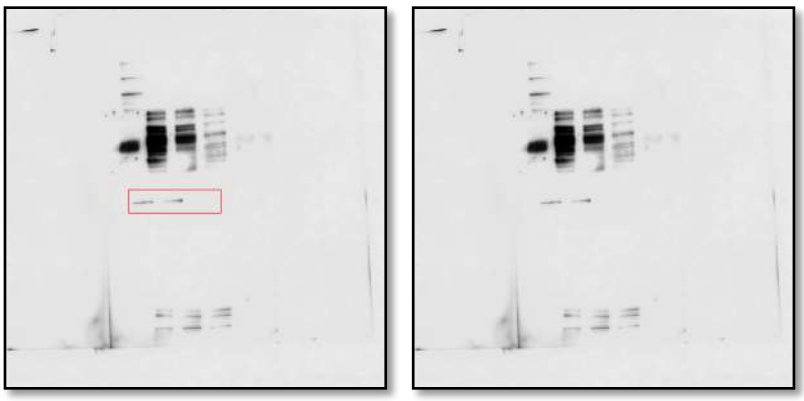

Western blot analysis of Vimentin protein levels in either vehicle or Pizotifen-treated MDA-MB-231 cells or E-cadherin positive cells in Pizotifen-treated MDA-MB-231 cells.

Figure 5D_MMP1_source data

Western blot analysis of MMP1 protein levels in either vehicle or Pizotifen-treated MDA-MB-231 cells or E-cadherin positive cells in Pizotifen-treated MDA-MB-231 cells.

Figure 5D_MMP3_source data

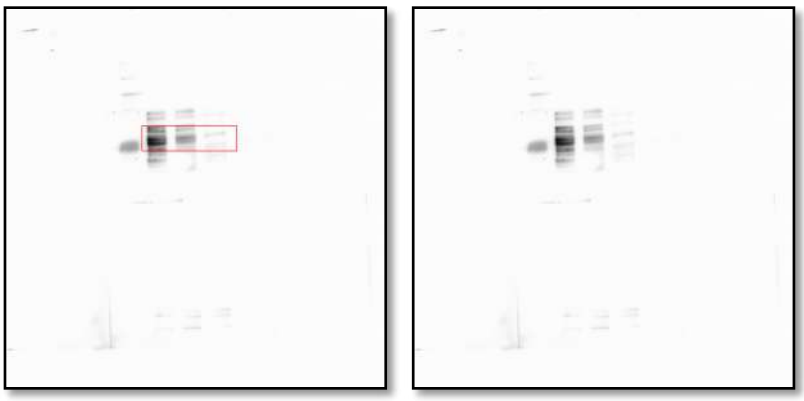

Western blot analysis of MMP3 protein levels in either vehicle or Pizotifen-treated MDA-MB-231 cells or E-cadherin positive cells in Pizotifen-treated MDA-MB-231 cells.

Figure 5D_S100A4_source data

Western blot analysis of S100A4 protein levels in either vehicle or Pizotifen-treated MDA-MB-231 cells or E-cadherin positive cells in Pizotifen-treated MDA-MB-231 cells.

Figure 5D_Zeb1_source data

Western blot analysis of Zeb1 protein levels in either vehicle or Pizotifen-treated MDA-MB-231 cells or E-cadherin positive cells in Pizotifen-treated MDA-MB-231 cells.

Figure 5D_GAPDH_source data

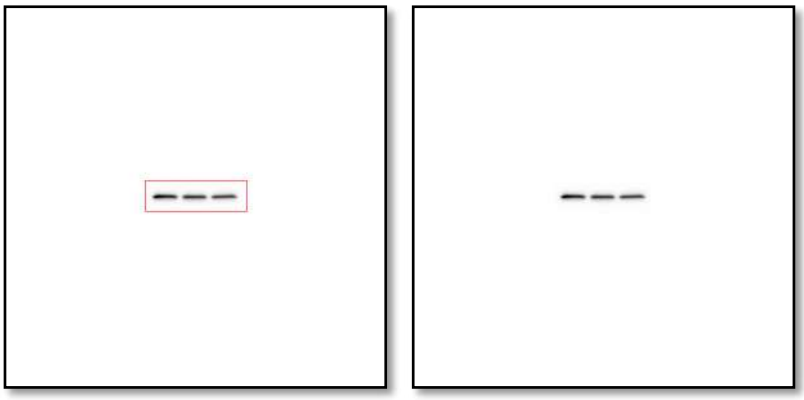

Western blot analysis of GAPDH protein levels in either vehicle or Pizotifen-treated MDA-MB-231 cells or E-cadherin positive cells in Pizotifen-treated MDA-MB-231 cells.

Figure 5F_β-catenin in the nucleus_source data

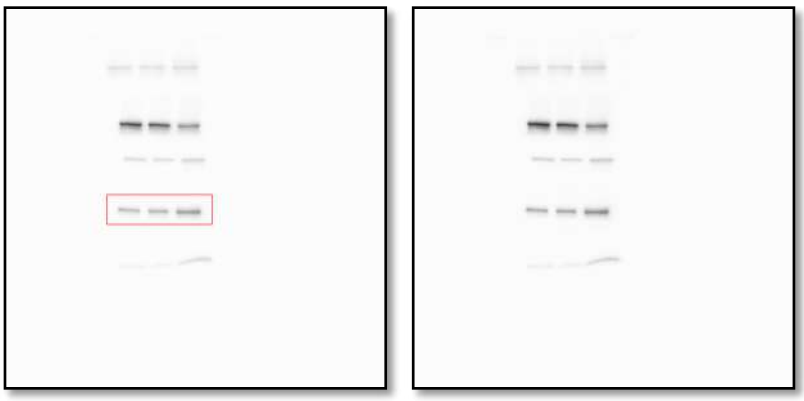

Western blot analysis of β-catenin protein levels in the nuclear of MCF7 cells expressing either the control vector or HTR2C.

Figure 5F_Histone H3 in the nucleus _source data

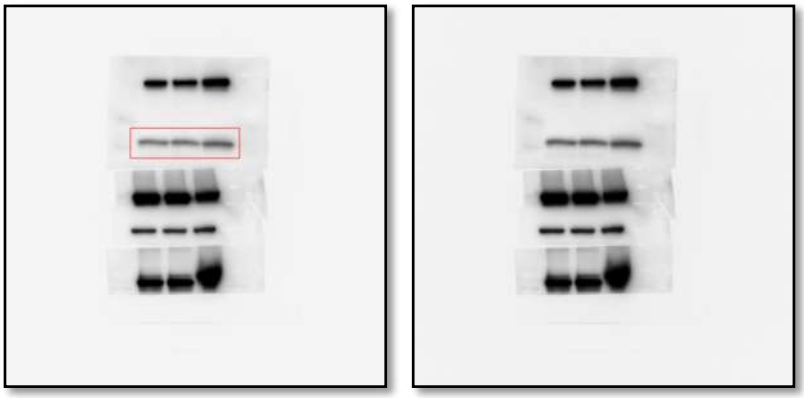

Western blot analysis of Histone H3 protein levels in the nuclear of MCF7 cells expressing either the control vector or HTR2C.

Figure 5F_β-catenin in the cytoplasm_source data

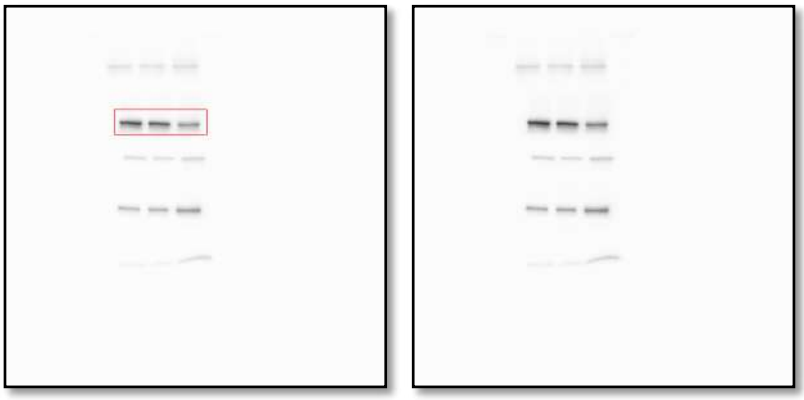

1225 Western blot analysis of β-catenin protein levels in the cytoplasm of MCF7 cells

1226 expressing either the control vector or HTR2C.

1227

1228 **Figure 5F_β-tubulin in the cytoplasm_source data**

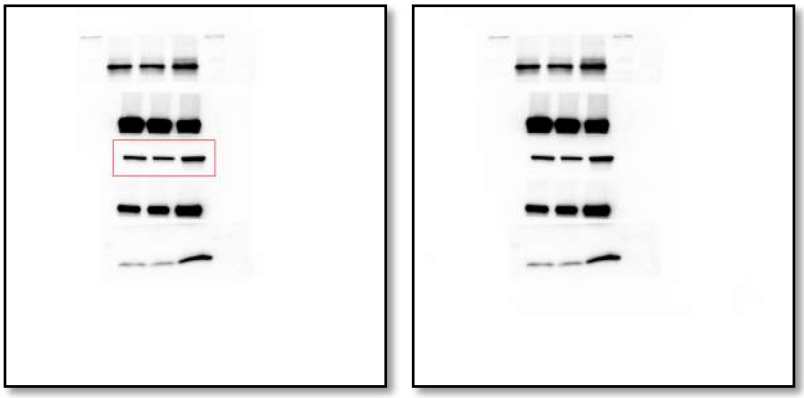

1229

1230 Western blot analysis of β-tubulin protein levels in the cytoplasm of MCF7 cells

1231 expressing either the control vector or HTR2C.

1232

1233 **Figure 5F_Phosphorylation of serine-9 in GSK3β_source data**

1234

1235 Western blot analysis of the protein levels of phosphorylation of serine-9 in GSK3β in

1236 whole cell lysate of MCF7 cells expressing either the control vector or HTR2C.

1237

1238 **Figure 5F_GSK3β_source data**

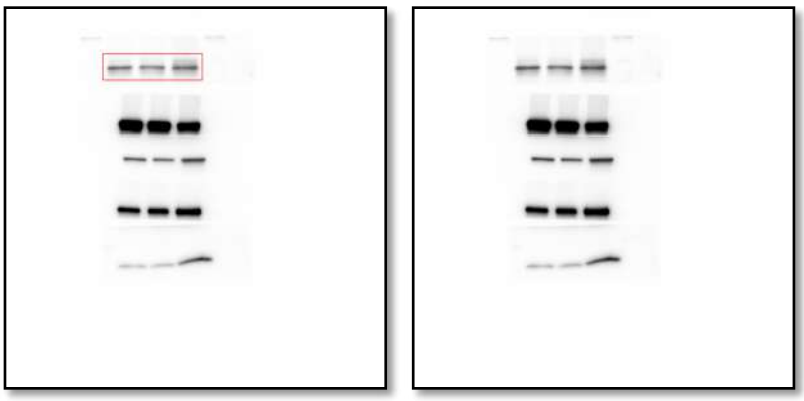

Western blot analysis of GSK3β protein levels in whole cell lysate of MCF7 cells expressing either the control vector or HTR2C.

Figure 5F_GAPDH_source data

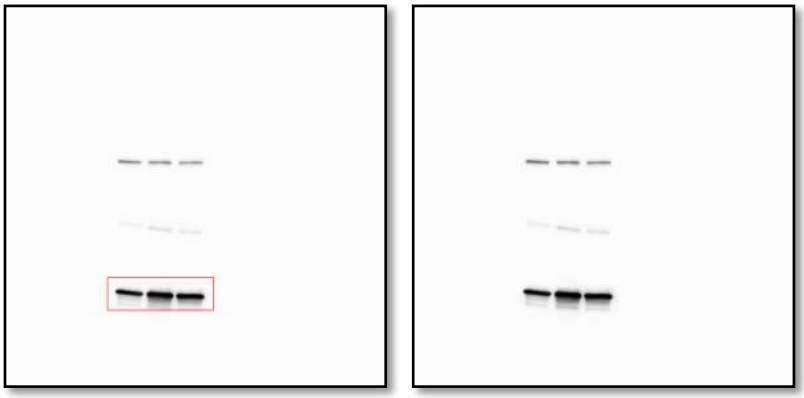

Western blot analysis of GAPDH protein levels in whole cell lysate of MCF7 cells expressing either the control vector or HTR2C.

Figure 5H_β-catenin in the nucleus_source data

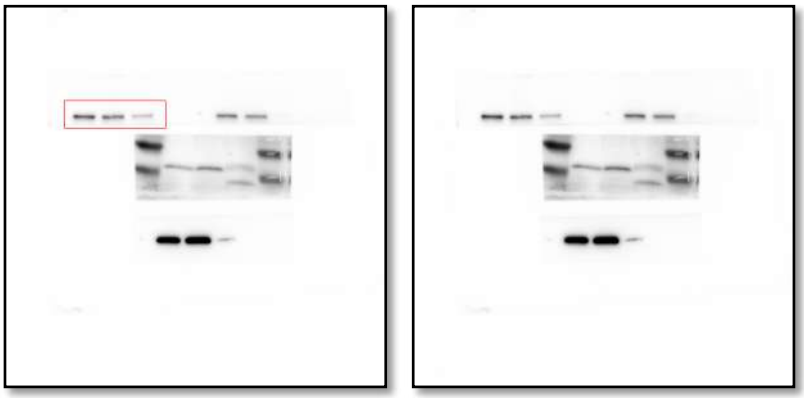

1250 Western blot analysis of β-catenin protein levels in the nucleus of either vehicle or

1251 Pizotifen-treated MDA-MB-231 cells or E-cadherin positive cells in Pizotifen-treated

1252 MDA-MB-231 cells.

1253

1254 **Figure 5H_Histone H3 in the nucleus _source data**

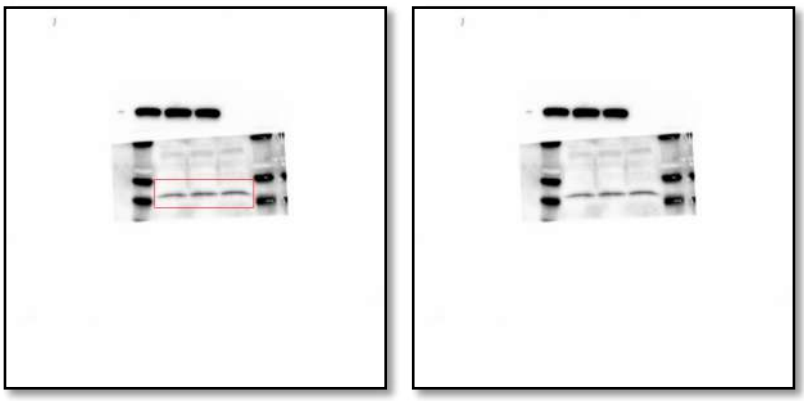

1255

1256 Western blot analysis of Histone H3 protein levels in the nucleus of either vehicle or

1257 Pizotifen-treated MDA-MB-231 cells or E-cadherin positive cells in Pizotifen-treated

1258 MDA-MB-231 cells.

1259

1260 **Figure 5H_β-catenin in the cytoplasm_source data**

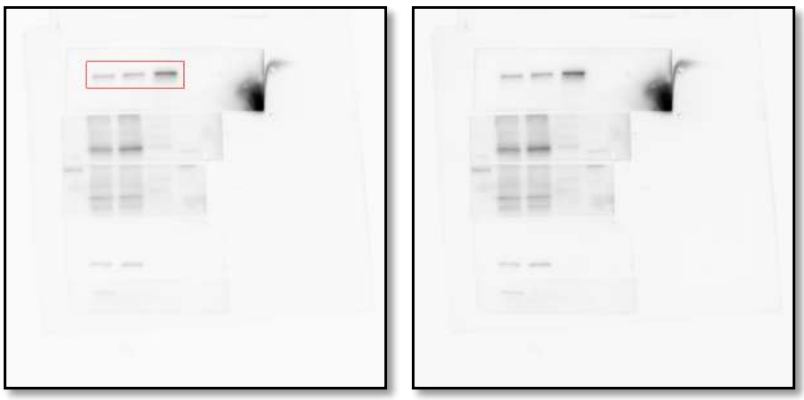

1261

1262 Western blot analysis of β-catenin protein levels in the cytoplasm of either vehicle or

1263 Pizotifen-treated MDA-MB-231 cells or E-cadherin positive cells in Pizotifen-treated

1264 MDA-MB-231 cells.

1265

1266 **Figure 5H_β-tubulin in the cytoplasm_source data**

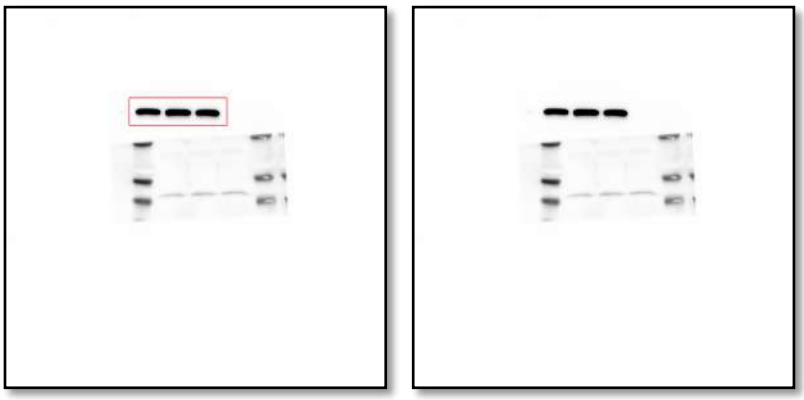

1267

1268 Western blot analysis of β-tubulin protein levels in the cytoplasm of either vehicle or

1269 Pizotifen-treated MDA-MB-231 cells or E-cadherin positive cells in Pizotifen-treated

1270 MDA-MB-231 cells.

1271

1272 **Figure 5H_Phosphorylation of serine-9 in GSK3β_source data**

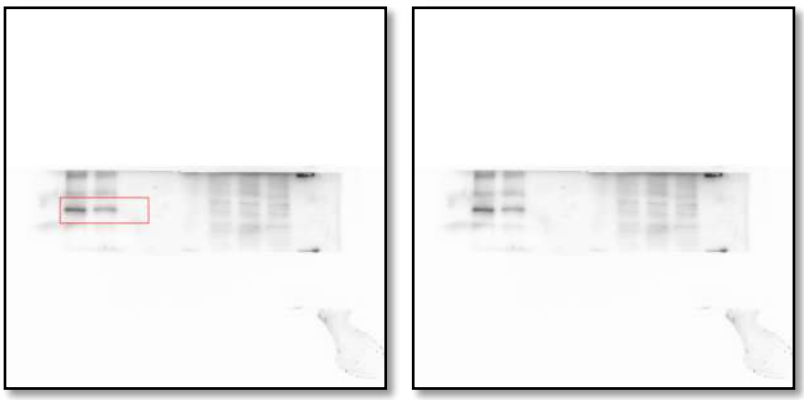

1273

1274 Western blot analysis of the protein levels of phosphorylation of serine-9 in GSK3β in

1275 whole cell lysate of either vehicle or Pizotifen-treated MDA-MB-231 cells or E-

1276 cadherin positive cells in Pizotifen-treated MDA-MB-231 cells.

1277

1278 **Figure 5H_GSK3β_source data**

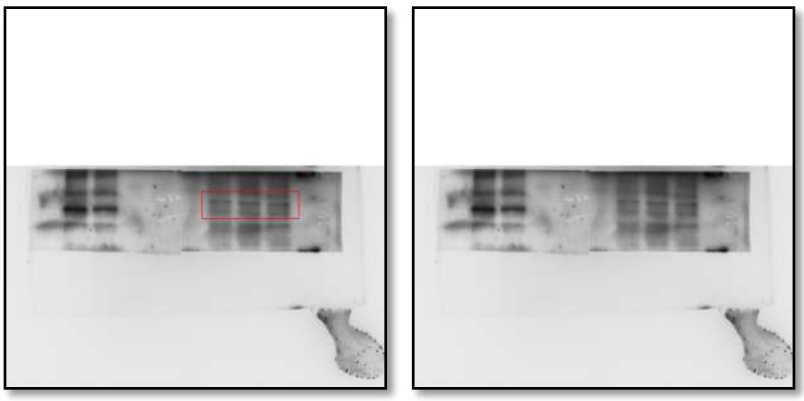

Western blot analysis of GSK3β protein levels in whole cell lysate of either vehicle or Pizotifen-treated MDA-MB-231 cells or E-cadherin positive cells in Pizotifen-treated MDA-MB-231 cells.

Figure 5H_GAPDH_source data

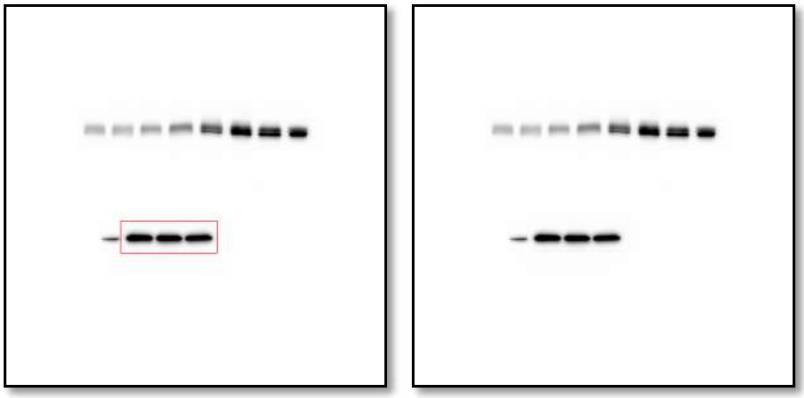

Western blot analysis of GAPDH protein levels in whole cell lysate of either vehicle or Pizotifen-treated MDA-MB-231 cells or E-cadherin positive cells in Pizotifen-treated MDA-MB-231 cells.

Figure S1A_ PRMT1_source data

1291 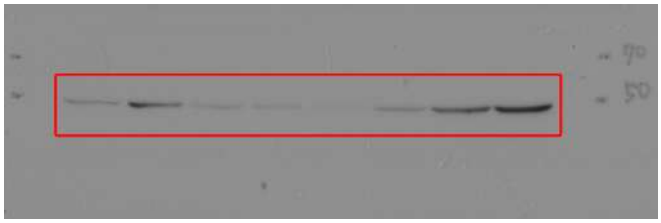

1292 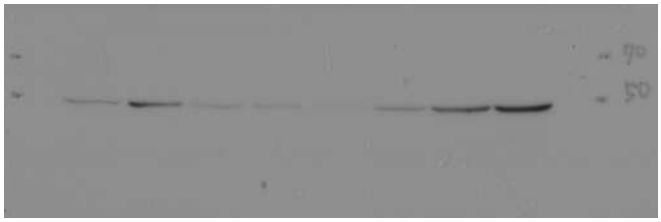

1293 Western blot analysis of PRMT1 protein levels in non-metastatic human cancer cell

1294 line (MCF7) and highly metastatic human cancer cell lines (MDA-MB-231, MDA-

1295 MB-435, MIA-PaCa2, PC9, HCCLM3, SW620 and PC3).

1296

1297 **Figure S1A_ CYP11A1_source data**

1298 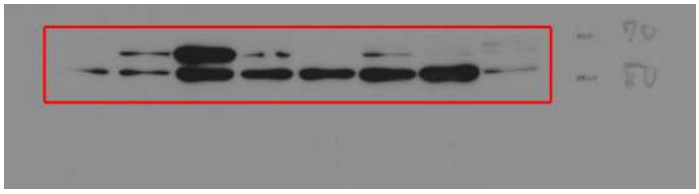

1299 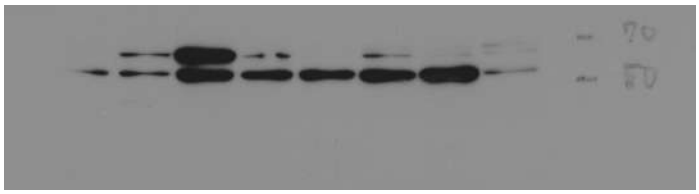

1300 Western blot analysis of CYP11A1 protein levels in non-metastatic human cancer cell

1301 line (MCF7) and highly metastatic human cancer cell lines (MDA-MB-231, MDA-

1302 MB-435, MIA-PaCa2, PC9, HCCLM3, SW620 and PC3).

1303

1304 **Figure S1A_ β-actin_source data**

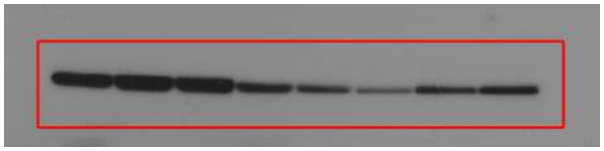

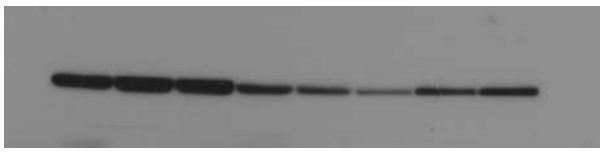

Western blot analysis of β-actin protein levels in non-metastatic human cancer cell line (MCF7) and highly metastatic human cancer cell lines (MDA-MB-231, MDA-MB-435, MIA-PaCa2, PC9, HCCLM3, SW620 and PC3).

Figure S1A_ PRMT1_source data

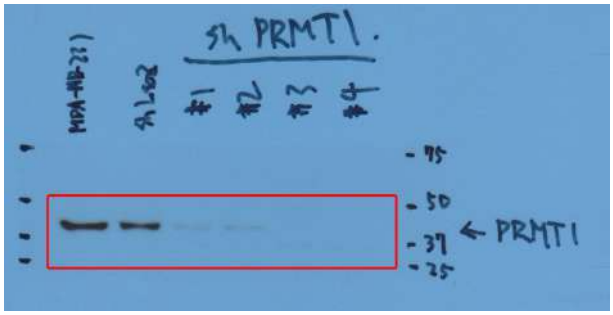

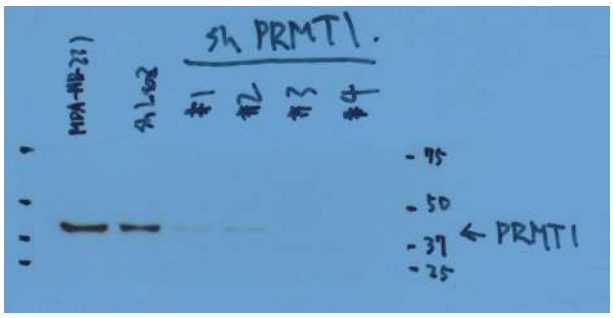

Western blot analysis of PRMT1 protein levels in sub-clones of MBA-MB-231 cells which were transfected with either a control shRNA targeting LacZ or one of four independent shRNAs targeting PRMT1 (clone #1 to #4).

Figure S1A_ β-actin _source data

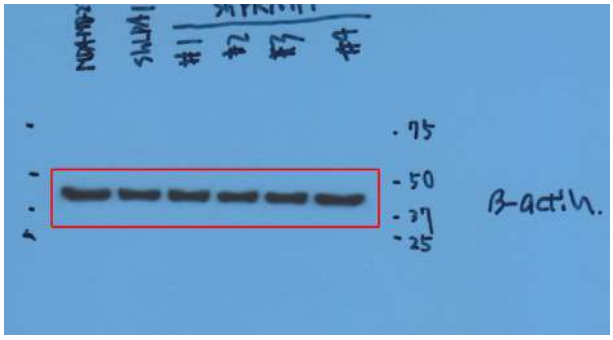

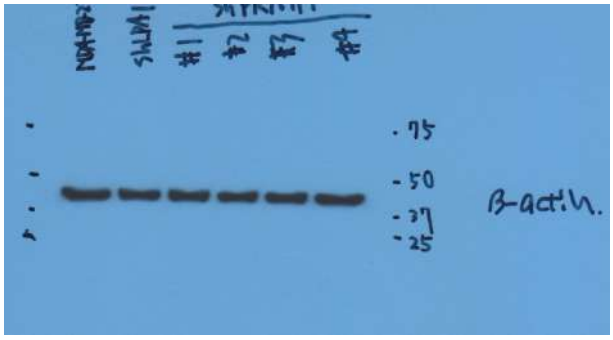

Western blot analysis of β-actin protein levels in sub-clones of MBA-MB-231 cells which were transfected with either a control shRNA targeting LacZ or one of four independent shRNAs targeting PRMT1 (clone #1 to #4).

Figure S1A_CYP11A1_source data

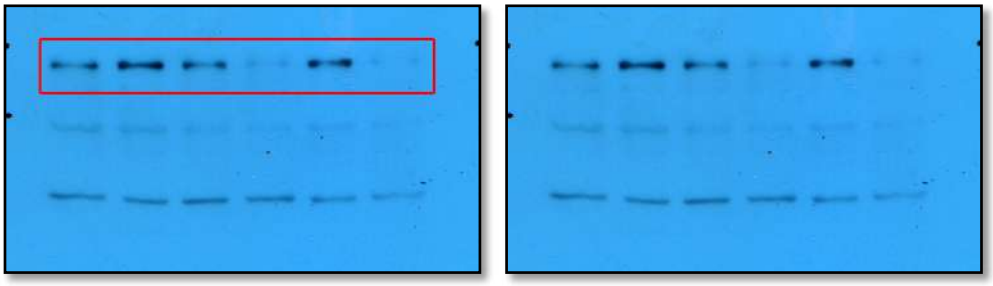

Western blot analysis of CYP11A1 protein levels in sub-clones of MBA-MB-231 cells which were transfected with either a control shRNA targeting LacZ or one of four independent shRNAs targeting CYP11A1 (clone #1 to #4).

Figure S1A_ β-actin_source data

1332 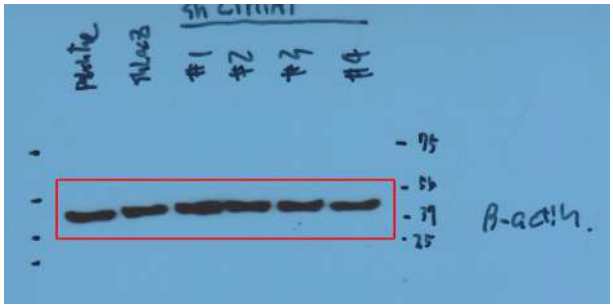

1333 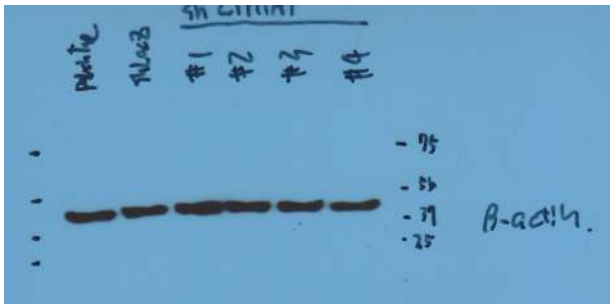

1334 Western blot analysis of β-actin protein levels in sub-clones of MBA-MB-231 cells

1335 which were transfected with either a control shRNA targeting LacZ or one of four

1336 independent shRNAs targeting CYP11A1 (clone #1 to #4).

1337

1338 **Figure S2A_DRD2_source data**

1339

1340 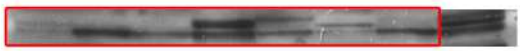

1341 Western blot analysis of DRD2 protein levels in non-metastatic human cancer cell

1342 line, MCF7 (breast) and highly metastatic human cancer cell lines, MDA-MB-231

1343 (breast), MDA-MB-435 (melanoma), MIA-PaCa2 (pancreas), PC3 (prostate) and

1344 SW620 (colon)

1345

1346 **Figure S2A_GAPDH_source data**

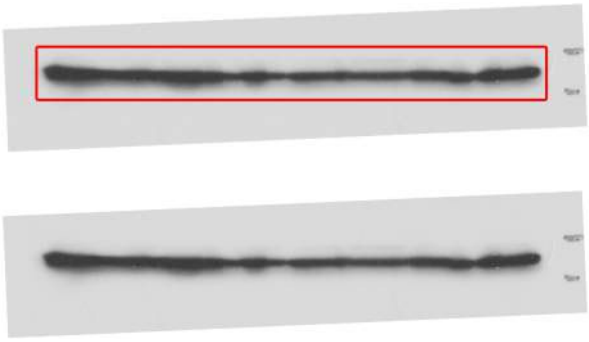

Western blot analysis of GAPDH protein levels in non-metastatic human cancer cell line, MCF7 (breast) and highly metastatic human cancer cell lines, MDA-MB-231 (breast), MDA-MB-435 (melanoma), MIA-PaCa2 (pancreas), PC3 (prostate) and SW620 (colon)